ROLE OF ISOSPIN MOMENTUM DEPENDENT INTERACTIONS IN MULTIFRAGMENTATION OF MASS ASYMMETRIC COLLIDING NUCLEI

Dissertation submitted for the partial fulfilment of requirement for
The award of the degree of

Master of Science
In
Physics

Submitted by
Ramandeep Kaur
Roll no. 301204009
Under the guidance of
Dr. Suneel Kumar

School of physics and Material Science
Thapar University
Patiala – 147004 (PUNJAB)

CERTIFICATE

*I hereby declared that the report entitled "**Role of isospin momentum dependent interactions in multifragmentation of mass asymmetric colliding nuclei**" is an authentic record of my own work carried out for the partial fulfillment of the requirement for the award of the degree of **M.Sc. (Masters of Science)** at Thapar University, Patiala (Punjab), under the guidance of Dr. Suneel Kumar, Associate Professor, School of Physics and Materials Science. The matter presented in the dissertation has not been submitted in part or full for the award of any other degree.*

Ramandeep Kaur

Date: 10/07/2014

Ramandeep Kaur

Roll No. :301204009

It is certified that the above statement made by the candidate is correct to the best of my knowledge and belief.

S Kumar

Dr. Suneel Kumar

Associate Professor
School of Physics and Materials Science
Thapar University, Patiala

(Dr. Kulvir Singh)

Professor
Head
School of Physics and Materials Science
Thapar University, Patiala

(Dr. S.K. Mohpatra)

Senior Professor
Dean of Academic Affairs
Thapar University,
Patiala

ACKNOWLEDGEMENT

Foremost, I would like to express my sincere gratitude to my supervisor **Dr. Suneel Kumar** for his continuous support and supervision, for his patience, motivation, enthusiasm, and immense knowledge. His guidance helped me at all times of research and in writing this dissertation. I could not have imagined having a better advisor and mentor for my thesis.

I would like to thank **Dr. Kulvir Singh**, Head, School of Physics and Materials Science for his support and providing me the necessary lab facilities.

I express words of thanks from the bottom of my heart to **Miss Navjot Kaur Virk**, without whom I would not have been able to complete my dissertation. My sincere thanks to the research scholars of the physics department for their help and valuable suggestions.

I am deeply thankful to my family, for their moral support and patience which gave me the necessary motivation and strength to endure research and complete my thesis.

Above all I render my gratitude to Almighty who bestowed me the strength and vision to walk on the path of truth.

I would like to acknowledge the financial support provided by the Department of Atomic Energy (DAE), Government of India, vide sanction No. 2012/37P/16/BRNS.

Date: 10/07/2014

Ramandeep Kaur

Place: Thapar University, Patiala

Roll No. 301204009

List of Publications:

a. Isospin effects of momentum dependent interactions in multifragmentation of asymmetric collisions.

   Navjot Kaur Virk, Ramandeep Kaur and Suneel Kumar

   Proc. 75-years of Nuclear Fission: Present Status and Future Perspectives, May 8-10, 2014, Pg. No. **110.**

b. Role of isospin momentum dependent interactions in multifragmentation of mass asymmetric colliding nuclei.

   Navjot Kaur Virk, Ramandeep Kaur, Suneel Kumar, Rajeev Kumar Puri, and Sailajananda Bhattacharya (to be submitted)

Contents **Page No.**

Chapter 1: Introduction

Chapter 2: Methodology

Chapter 3: Effect of isospin dependent momentum interactions (IMDI) on multifragmentation of mass asymmetric colliding nuclei

ABSTRACT

The main motive of the present thesis is to investigate the contribution of isospin momentum dependent interactions in the multifragmentation of asymmetric colliding nuclei, in which the mass of target nuclei is fixed and the mass of projectile nuclei is varied. These different combinations of projectile and target nuclei have been simulated within the framework of Isospin Quantum Molecular Dynamics model (IQMD) and IQMD (Th01) model for the respective momentum dependent and isospin momentum dependent interactions. The results clearly signifies the importance of isospin momentum dependent interactions for asymmetric colliding pairs. Thus, the isospin dependence of momentum dependent interactions should be taken into account for the various studies related to highly asymmetric reactions.

Chapter 1

INTRODUCTION

The science of nuclear physics deals with the properties of "nuclear matter" which makes up the massive centers of the atoms accounting 99.95 % of the matter. The main attention is subjected to the structure of nuclei, interaction among nucleons (i.e. protons and neutrons), nucleon-nucleon scattering, as well as the structure of nucleons. Nuclear physics apart from a subject of basic research also makes a remarkable contributions to the needs of society, in terms of nuclear energy, nuclear medicine, ion implantation in materials engineering, and radiocarbon dating in geology and archaeology etc. It also explores the heavy nucleus-nucleus collisions which is of relevance not only for nuclear physics, but also for the astrophysical research [1]. Let us now review some of the features of heavy-ion physics.

1.1 HEAVY ION PHYSICS

The particle with mass number greater than or equal to the mass of alpha particle is known as heavy ion. Heavy ion collisions (HICs) are of great importance to understand many properties of nuclear matter, such as nuclear radii, nuclear structure, nuclear density, binding energy, different shapes of nuclei, interactions among nucleons (protons and neutrons) and nucleon-nucleon scattering.

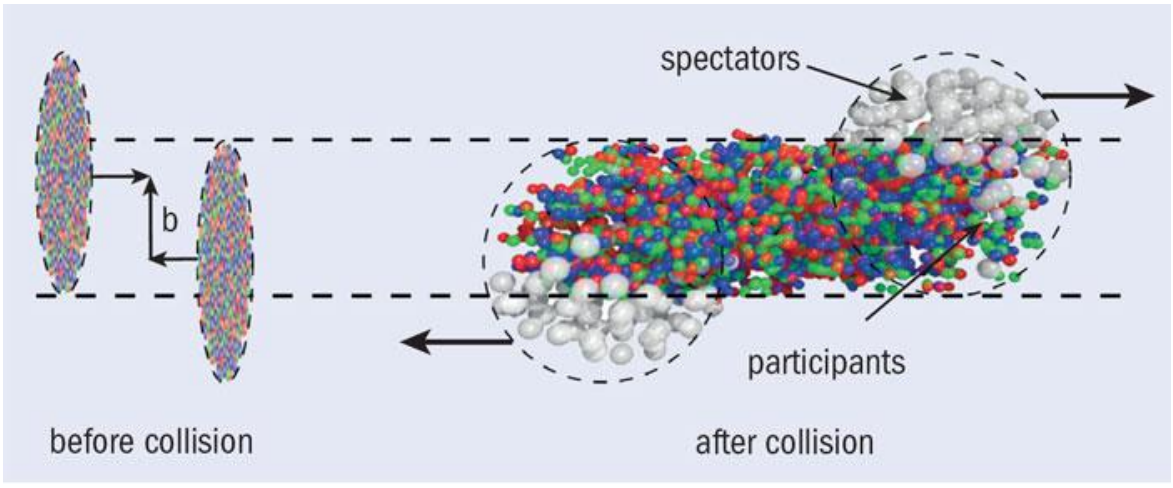

Fig.1.1: Schematic view of the Heavy ion collisions

Fig.1.1 shows the heavy ion dynamics before and after the collision. HICs at intermediate and high energies creates a compressed state of matter at extreme conditions of density and

temperature. HICs serves a purpose for understanding the nuclear matter in those conditions which are different from those in normal nuclei, such as density, as in this state the density becomes 2-3 times the normal nuclear matter density and temperature. This type of knowledge is also useful in astrophysics to understand the formation of neutron stars, supernova explosions and the evolution of the early universe [2].

On the basis of the energy of the two colliding nuclei, heavy ion physics can be classified in the following branches:

1. Low energy HICs: $E < 10$ MeV/nucleon
2. Intermediate energy HICs: 10 MeV/nucleon $\leq E \leq 2$ GeV/nucleon
3. High energy HICs: $E > 2$ GeV/nucleon

1.1.1 LOW ENERGY HICs

This energy range deals with the nuclear interactions, fusion-fission, cluster radioactivity, synthesis of super heavy elements and halo nuclei etc [3]. In other words, the low energy concentrates mainly on the structure of the nucleus. The reaction cross-section at low incident energies consist of three categories namely, the fusion, quasi-elastic and deep inelastic scattering. All these processes depend upon the angular momentum of projectile and at incident energy. At this range of energy, the colliding nuclei cannot compress completely with each other, therefore due to the lack of free phase space, 98% of the collisions are blocked. Here, nucleon-nucleon collisions are negligible and only the mean field plays a dominant role.

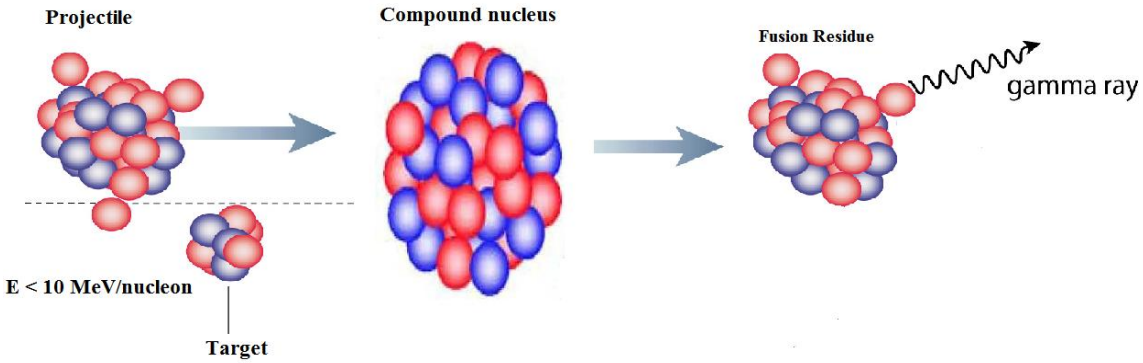

Fig.1.2 Schematic view of fusion at low energy (E < 10 MeV/nucleon)

1.1.2 INTERMEDIATE ENERGY HICs

In this energy range, both mean field and nucleon-nucleon collisions play an important role. In this energy range, maximum density achieved is equal to 2-3 times the normal nuclear matter density. In this range, the compressibility and the nature of nuclear equation of state (NEoS) can be investigated. Due to the formation of compressed nuclear matter at intermediate energies, there is a possibility to study the properties of nuclear matter at extreme conditions of density and temperature. This range investigates the behaviour of hadrons, multi-fragmentation, nuclear stopping and collective flow etc. [4,5]. Fig.1.3 shows the schematic view of fragmentation process at intermediate energy 100 MeV/nucleon. Reactions at intermediate energy range are violent enough to excite the system to very high temperature and density, that leads to the breakup of initial correlations among nucleons, but not enough to break the internal structure of nucleons or hadrons.

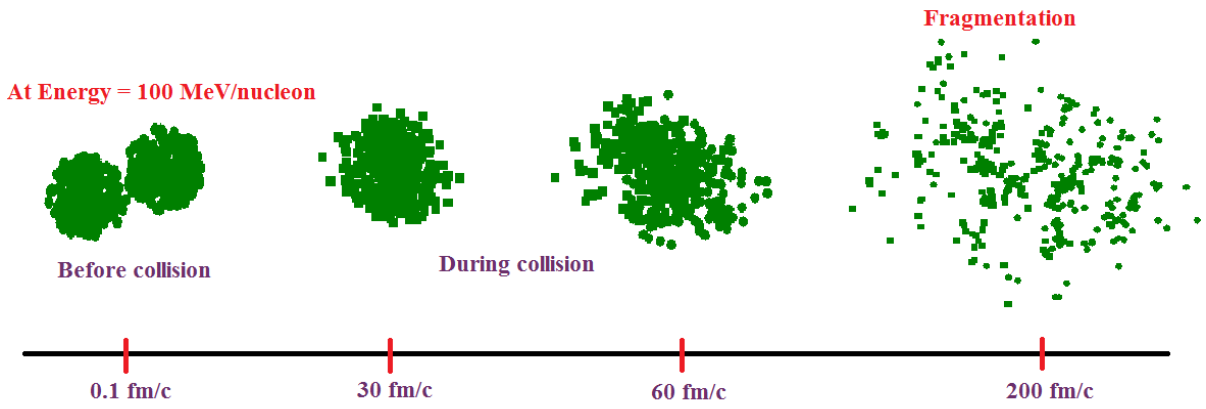

Fig.1.3 Schematic view of multifragmentation at intermediate energy (100 MeV/nucleon)

1.1.3 HIGH ENERGY HICs

High energy HICs deals with the properties of nuclear matter at energies greater than 2 GeV/nucleon. Fig.1.4 shows a schematic view of collision at high energy 5 GeV/nucleon. In this range, the density and temperature is very high compared to normal nuclear matter. A highly hot and dense region represents the quark gluon plasma (QGP). In this range, the phenomena of particle production is usually studied. In this energy range, due to the availability of larger free space, only few collisions (4%) are blocked and hence Pauli blocking plays the negligible role in this range. The reaction dynamics at this energy is mainly governed by the nucleon-nucleon collisions [6], which are able to break the internal

structure of a nucleon.

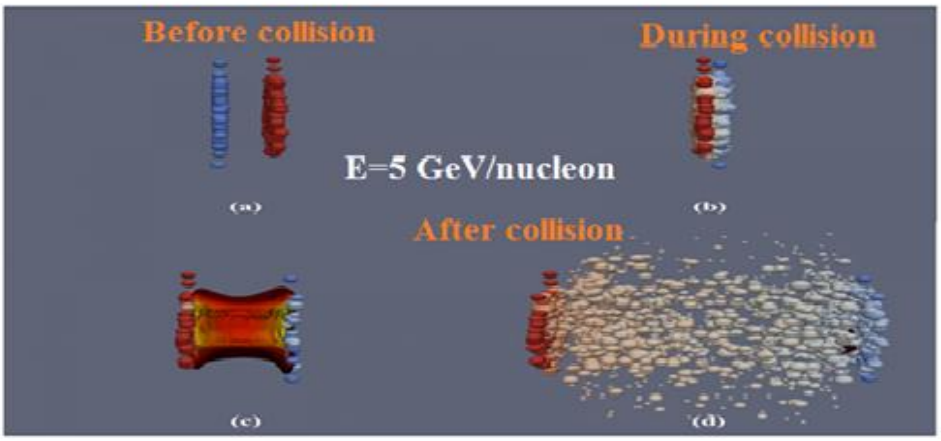

Fig.1.4 Schematic view of particle production at high energy (5GeV/nucleon)

1.2 PHASE DIAGRAM OF NUCLEAR MATTER

The nuclear matter produced from the HICs is being studied to understand the early history of the universe, and to understand the highly dense objects, called "neutron stars" that exist in the present day universe. At higher densities and temperatures, system undergoes a transition in their phase.

In normal states at lower energy, nuclei show liquid-like characteristics. At this energy, density is 0.17 nucleons/fm^3. In more conventional units, this is equals to 2.7 X 10^{17} kg/m^3, or 270 trillion times the density of liquid water. In Fig.1.5, the phase diagram of nuclear matter is displayed. The normal nuclear matter at T = 0 and $\rho = \rho_0$ represents a liquid phase.

The liquid gas phase (LGP) transistion region at the lower left corner of the Fig.1.5 is shown by the temperature less ≈ 15 MeV and densities $\rho/\rho_0 < 1$. The region of extremely high temperature and density represents the QGP phase. The hadron gas (HG) phase is present at intermediate densities and temperatures. The neutron star region extends from low density upto more than 10 times the normal nuclear matter density. The two lines that separate the QGP phase from the HG phase is the transition region [7].

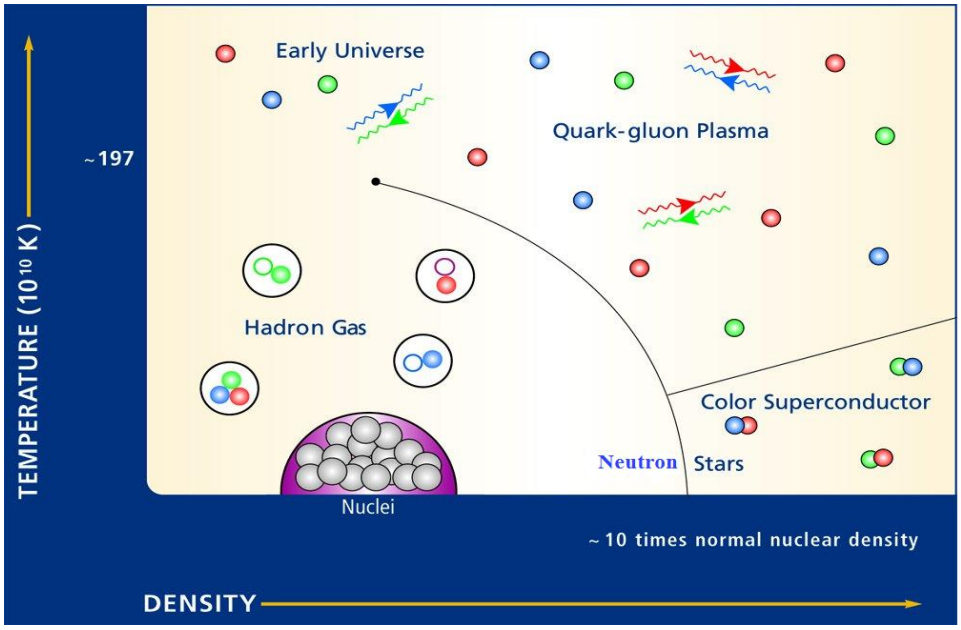

Fig.1.5 The phase diagram for nuclear matter, as predicted theoretically. The horizontal axis shows the scaled density, and the vertical axis shows the temperature.

The main purpose of studying the nuclear matter phase diagram is to understand the astrophysical phenomena which helps in understanding the history of early universe. Depending on the temperature and densities, large scale investigation of the nuclear matter phase diagram is possible. Other regions like the neutron stars as well as supernova explosions are remote in time and far in space so, are of limited interest only. The region that provides information about nuclear matter and phase diagram under the extreme conditions is the HICs at intermediate energies. It offers an excellent possibility to study various phenomena such as nucleon-nucleon collisions, multi-fragmentation, collective flow and nuclear stopping etc. The specific region of the phase diagram and its related physics depends mainly on the incident energy of the system. Reactions at intermediate energies are vicious enough to excite the system to very high temperature that leads to the break-up of initial correlations among nucleons, but this temperature is not enough to break the internal structure of nucleons or hadrons. Therefore, HICs offers a unique opportunity to search the phase diagram also. It has been mentioned in [8] that the choice of the projectile in case of multifragmentation is responsible for 10 to 50% of the reaction cross-section. Furthermore, multifragmentation opens a unique opportunity for investigating the phase diagram of nuclear matter at densities around $\rho \approx 0.1\rho_0 - 0.3\rho_0$ (where, $\rho_0 \approx 0.17$ fm^{-3} denotes the normal nuclear matter density) and temperature T≈3-8 MeV.

1.3 NUCLEAR EQUATION OF STATE

NEoS played a central role in hot and dense nuclear matter physics, which shows a nontrivial relation between the thermodynamical variables such as between pressure P and baryon density ρ , between temperature T, P(ρ,T) and chemical potential T, P(μ,T), between energy density e, ρ and T, e(ρ,T), etc which characterize the medium. NEoS gives the information about how much the nuclear matter can be compressed at a given energy. The nuclear matter can be compressed by colliding two nuclei; it means that the compressional energy is added to the system. NEoS informs us that which compressional energy corresponds to which density. The NEoS is of interest, because it affects the fate of the universe at times $t \geq 1\mu s$ from the Big Bang and its features are behind the supernova explosions. Moreover, its features ensure the stability of neutron stars and tells about the supernova collapse [2].

The next nontrivial feature of the energy per nucleon is its curvature in the dependence on ρ , around ρ_0. This curvature is commonly quantified in terms of the factor, called as nuclear incompressibility, which is defined as [5]

$$K = 9\rho_0^2 \frac{\partial^2 W}{\partial \rho^2} \tag{1}$$

The value of K ranges from about 200 MeV, which is less repulsive and known as soft equation of state (EoS), up to about 400 MeV, which is more repulsive and known as hard EoS. The corresponding compressional energy curves are shown in Fig.1.6.

Apart from different EoS, the momentum dependence of EoS has also attracted lot of concentration. From the reference [9], it should be noted that the compressibility depends not only on the density but also on the entire momentum plane. In other words, EoS not only depends on the population of nucleons but also depends upon their relative velocities. These momentum dependent interactions (MDIs), give rise to two new equations of state. A set with momentum dependence and soft EoS is called SMD, whereas a hard EoS with momentum dependence is called HMD. Out of the various phenomena which are being studied at intermediate energy HICs, multifragmentation is one of the important phenomena, which is discussed in the next section.

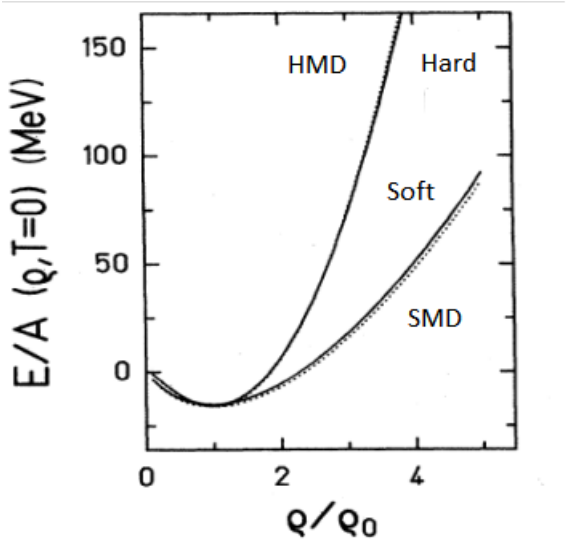

Fig.1.6 The density dependence of the compressional energy per particle. The hard, soft, hard momentum dependent (HMD) and soft momentum dependent (SMD) interactions are shown by solid, dash-dot-dash, dash-double-dotted and dashed lines, respectively. This Figure is taken from reference [5].

1.4 MULTIFRAGMENTATION

The crushing of the colliding nuclei into pieces leads to the phenomenon of multifragmentation. After the collision, the nuclear matter undergoes a phase transition. The highly compressed and concentrated nuclear matter gets condensed by the emission of large number of fragments as shown in Fig.1.7. The fragments are classified as free nucleons (FN's) [A = 1], light mass fragments (LMF's) [2 ≤ A ≤ 4], medium mass fragments (MMFs) [5≤A≤9], intermediate mass fragments (IMFs) [5≤A≤$A_{tot/6}$] as well as heavy mass fragments (HMFs) [21≤A≤$A_{tot/6}$]. The multifragmentation is an interesting process where one is interested to know the reason of this break up that it is a statistical process, making micro canonical phase space model a proper tool or it is driven by the fluctuations during the reaction [10]. A schematic view of the multifragmentation is illustrated in Fig.1.7.

The Fig. 1.7 shows that at intermediate energy, two nuclei collide to form a highly compressed nuclear matter and then decompose into small, medium and large size fragments. This compressed nuclear matter gives information about the nuclear matter under extreme conditions. Multifragmentation is a universal phenomena which takes place when a substantial amount of energy is transferred from one nucleus to the other nucleus. This

process has been observed in nearly all types of high energy nuclear reactions induced by photons, heavy ions and hadrons. During the initial phase of the reaction compression in the

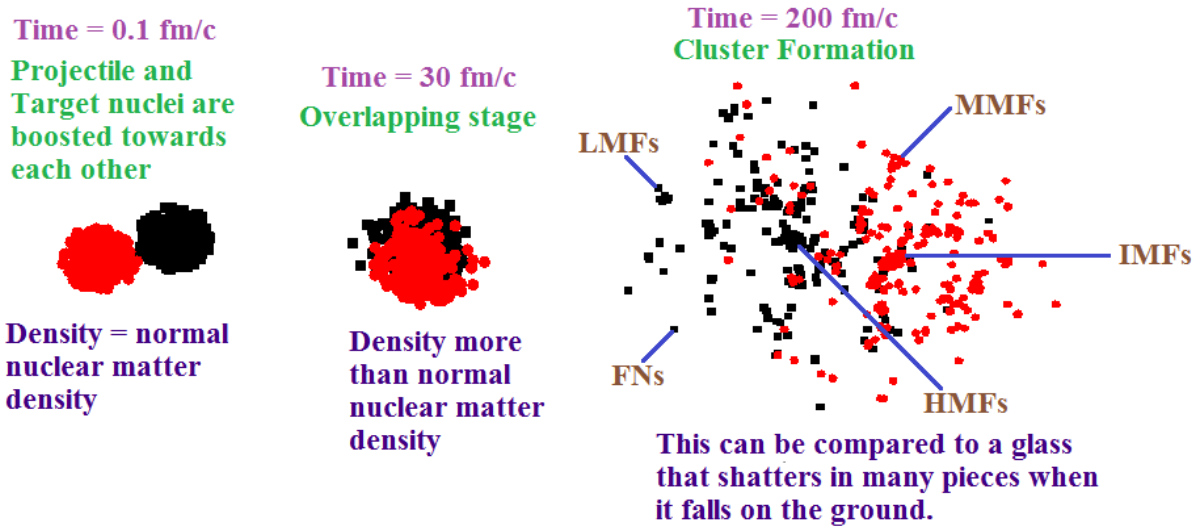

Fig.1.7 Two nuclei collide to form a compressed matter and then fragmented.

system exists and due to the high excitation energy, the system will expand to subsaturation densities, becoming unstable compressed matter and then break up into many fragments. Multifragmentation is a fast process with characteristic time less than or around 100 fm/c. The detailed analysis of the fragmentation process on the experimental and theoretical front revealed that the fragmentation depends crucially on the impact parameter, incident energy, total mass, isospin asymmetry and the mass asymmetry of the colliding nuclei [11]. The mass asymmetry is explained in the next section.

1.5 MASS ASYMMETRY

The HIC's include two types of reaction, mass symmetric and mass asymmetric reactions. Mass symmetric reactions are those in which there are equal number of neutrons and protons in the projectile and target nuclei. On the other hand, the mass asymmetric reactions are those in which number of neutrons and protons are not equal in the projectile and target nuclei.
The mass asymmetry parameter (η) can be defined as [9],

$$\eta = \frac{A_T - A_P}{A_T + A_P} \qquad (2)$$

where, A_T and A_P are the masses of target and projectile nuclei respectively.

The $\eta = 0$ corresponds to the mass symmetric reactions, whereas non-zero values of η corresponds to the mass asymmetric reactions. The distribution of nucleons is symmetric for mass symmetric reactions in the reaction plane, whereas for the mass asymmetric reactions, the distribution is asymmetric in the reaction plane.

The mass asymmetry of the colliding nuclei also effects the production of fragments. In the asymmetric colliding nuclei, the heavier mass (A^{max}) continuous to grow and close to the sum of mass of colliding nuclei. In contrast, the production of FNs, LMFs and IMFs shows a opposite trend as compared to A^{max}, which comes into picture due to the decrease in the participant zone [12]. For the present objective, asymmetric colliding nuclei have been taken into account in which the target is fixed but mass of the projectile is varied. Before moving further, various experimental and theoretical attempts made in the direction of mass asymmetric reactions have been reviewed in the next section.

1.6 REVIEW OF EXPERIMENTAL EFFORTS

Many experimental efforts have been made in studying the process of multifragmentation in HICs at intermediate energies. In the following, we shall present the review of this phenomena explained by different collaborations.

- The experiments performed in Berkley served a purpose for the intermediate energy HICs to probe the EoS. The Berkley group focuses mainly on the mass asymmetric reactions named as $^{197}Au+^{27}Al$, ^{51}V and ^{nat}Cu to investigate the role of entrance-channel mass asymmetry reaction dynamics. This group perform the reactions from the energy 50 to 110 MeV/nucleon to determine the role of mass asymmetry [13]. The emphasis was on different parameters like excitation energy, cross-section as well as velocity distribution etc.

- National Superconducting Cyclotron Laboratory (NSCL) of Michigan State University (MSU) also worked on the mass asymmetric $^{36}Ar+^{19}7Au$ reactions at energy 50 MeV/nucleon. In this the average multiplicity as well as the heaviest fragments are recorded. For both symmetric and asymmetric reactions, the isospin effects are studied by neutron-proton spectra double ratio, binding energy etc [14].

- Bowman *et al*. [15] study the multifragmentation for $^{129}Xe+^{197}Au$ at E=50 MeV/nucleon with a low threshold 4π detection systems. They examined the multifragmentation decay of this system as a function of multiplicity of charged particles. The results are compared with both statistical and dynamical models.

- The FOPI and ALADIN groups at GSI studied the multifragmentation for asymmetric reacting partners. They studied the multifragmentation process over a wide range of masses from ^{12}C to ^{208}Pb between the energies from 100 and 1000 MeV/nucleon. They showed the rise and fall in the multiplicity of intermediate mass fragments (IMFs) [16].

- The NIMROD collaboration at TAMU studied the dynamics of HICs in the Fermi energy range. These collisions proved to be very useful in preparing highly excited light nuclei [17]. The EoS of isospin asymmetric nuclear matter has been also studied by this collaboration. They also studied the emission of IMFs (Z>2) in ^{124}Sn, $^{124}Xe+^{124}Sn$ and ^{112}Sn at 28 MeV/nucleon [18].

- INDRA group at GANIL (France) analyze the variety of parameters in multifragmentation. They studied the system size effects, the role of system size in entrance channel as well as kinetic energy spectra and fragment velocity correlation in asymmetric reaction $^{124}Xe+^{nat}Sn$ at 50 MeV/nucleon [19].

- De Souza *et al*. [20] observed a linear increase in the multiplicity of IMFs for central collisions at energy E=110 MeV/nucleon by the use of a low-threshold 4π detector array. Tsang *et al*. [21] showed a rise and fall in the multiplicity of the IMFs with the framework of SIS at GSI for symmetric nuclei. Their study shows that, as one goes for low to high energies, the maximum value of the IMFs shifts from central to peripheral collisions.

- Another study in which L. Manduci *et al*. [22] analyzed the reaction $^{93}Nb+^{nat}Mg$ at the incident energy of 30 MeV/nucleon and observed that the fragmentation process is responsible for fragment production around the excitation energy of 3 MeV/nucleon.

- Experimental evidences for the statistical property of nuclear fragmentation has been made for reactions ^{197}Au projectile with different targets as C, Al, Cu. and various new quantities have been measured in ref. [23]. These quantities include the mean multiplicity of intermediate mass fragments $<N_{IMF}>$ ($5 \leq A \leq Atot/6$) ,the average charge of the largest fragment (Z_{max}), the sum of all charges with $Z \geq 2$ etc. The quantity which is intimately related to the multifragmentation process is the multiplicity of IMFs. The correlations between the $<N_{IMF}>$, and the mass of fragmenting system, whose measure is so called bound charge (Z_{bound}) and is an important aspect of the multifragmentation process that has been studied by many groups [23,24]. They also observed the rise and fall in the multiplicities of IMFs.

- C. William *et al*. [25] carried out experiment for central collision of ^{84}Kr+^{197}Au at the incident energy between 30 and 400 MeV/nucleon. They found the peak in the IMF production around 100 MeV/nucleon.

- One of the early attempts to study the multifragmentation was made by Jakobsson *et al*. [26], in which the charged particle distribution (along with their kinetic energy spectra) was measured for ^{16}O+^{36}Ar induced reaction between 25 MeV/nucleon and 200 MeV/nucleon representing the fusion, fission, particle emission, and multifragmentation.

1.7 REVIEW OF THEORETICAL EFFORTS

If the mass of projectile and target are comparably same, then reaction leads to high compression whereas, mass asymmetric reactions leads to the heat or thermal energy. In the theoretical treatment, there are many objectives before and after the collision in time scale on which the theory can be proposed. There are many theoretical attempts to study the multifragmentation process at intermediate energy, which can be explained as:

- Liu [27] studied the isospin effects on the process of multifragmentation and dissipation by considering the two pairs of asymmetric colliding nuclei ^{76}Zn+^{40}Ar and ^{76}Kr+^{40}Ca, ^{120}Cd+^{40}Ar and ^{120}Xe+^{40}Ca for central collisions.

- Y.K. Vermani *et al*. [28] studied the energy and mass dependence of fragment production with Quantum Molecular Dynamics (QMD) [29] model for mass symmetric as well as mass asymmetric reactions. Their results showed a linear mass dependence at the peak of centre of mass energy at which maximal IMF production occurs.

- Another study for the mass symmetric as well as mass asymmetric reactions was given by Sisan *et al*. [30]. They studied the emission of IMFs for central collisions and predicted a rise and fall in the emission of IMFs with beam energy for the reactions ^{40}Ar+^{45}Sc at energy 35-115 MeV/nucleon, ^{58}Ni+^{58}Ni at energy 35-105 MeV/nucleon and ^{86}Kr+^{93}Nb at energy 35-95 MeV/nucleon and observed a linear peak energy dependence on the size of the system.

- V. Kaur *et al*. [31] studied the fragmentation process by varying the mass asymmetry of the colliding nuclei from 0.2 to 0.7 at a fixed centre of mass energy. Their study predicts that, rise and fall in the multiplicity of IMFs observed for symmetric collisions, is reproduced nicely for the asymmetric collisions. However, this trend is missing for larger mass asymmetric colliding nuclei. Another study of the multifragmentation for the asymmetric colliding nuclei ${}^{16}_{8}O+{}^{136}_{54}Xe$, ${}^{128}_{14}Si+{}^{124}_{54}Xe$ [12] at different energies showed that LMFs originate from the mid-rapidity region and they are best suited for studying the effects of mass asymmetry on the reaction dynamics. This study is performed within an isospin-dependent quantum-molecular dynamics (IQMD) model [32]. In this study, the coulomb interactions were absent which enhance the production of fragments by 20%. In this study, they showed that nearly symmetric nuclei depict a well known trend i.e. the rise and fall around E=100 MeV/nucleon, but this trend is absent for larger asymmetric nuclei.

- J. Singh *et al.* [33] discuss the importance of momentum dependent interactions (MDI) in explaining the multifragmentation for mass asymmetric reactions named as O+Br. The reactions were simulated with the QMD model. They observed that MDI enhances the multiplicity of fragments for highly mass asymmetric reactions.

- Another study by J. Singh *et al*. [34] discuss the role of MDI and larger nucleon-nucleon cross section in multifragmentation using QMD model for mass asymmetric reactions. They predicted that the sensitivity of larger cross section towards the multifragmentation gets reduced in the presence of MDI.

Chapter 2

METHODOLOGY

Presently, many theoretical tools are also available to compare the various theoretical achievements with the experimental findings. The theoretical models make the situation more complicated. The key point to remember is that the HICs involve very complicated non equilibrium physics. Therefore, its understanding is not straight forward. The theoretical models at intermediate energy can be divided into two parts:

- Statistical models
- Dynamical models

The statistical models give a better description of the final stage of the reaction only. Example of the statistical model is statistical multifragmentation model (SMM) [35], which can incorporate specific nuclear properties directly. The dynamical models are very useful for studying the reaction from the initial state to the final state, where matter is fragmented and cold. Example of the dynamical models are Time Dependent Hartree-Fock (TDHF) approximation, first proposed by Dirac in 1930 [36].

The Hartree-Fock theory and Schrodinger equation are suitable for low energy reactions and have discussed the mean field theory [37]. The Cascade model [38] describes high energy HICs which takes into account only nucleon-nucleon collisions without taking Pauli-blocking into account. It neglects the mean field completely and do not take the isospin degree of freedom into account. To take the nucleon-nucleon collisions into account, Extended Time Dependent Hartree Fock Theory (ETDHF) [39] is used. Intra Nuclear Cascade [40] model is used for describing high energy HICs. This is the first microscopic model in which the mean field is neglected and nucleon-nucleon collisions are taken into account without considering Pauli-blocking. The microscopic transport model for one body Wigner phase space density distribution obtained by different names although they solve the same equation. Boltzmann-Uehling-Uhlenback equation (BUU) [41], which is used to study the large deviation problems of low, intermediate and relativistic high energy HICs. The BUU Model includes nucleon-nucleon collisions with the inclusion of Pauli Blocking. The BUU equation describes the time evolution of the one body distribution function. Event by event correlation cannot be analyzed with one body transport models. The BUU model is able to explain the one body observables like collective flow, stopping as well as particle spectra, while N body features

are not described by this model because the correlations and fluctuations are not preserved in this model. IBUU model [42] is the isospin version of the BUU model. In this model, isospin dependence has been incorporated by both the elementary nucleon-nucleon scattering cross section and the nuclear mean field. The Classical Molecular Dynamics (CMD) approach, which is an N-body theory, is capable of treating both the compression and fragment formation, but these calculations were done only on a completely classical level. Aichelin and Stocker, in 1991, introduced the quantum features like the Pauli principle, Stochastic scattering and particle production in a model which is dubbed as Quantum Molecular Dynamics (QMD) Model [29], and is based on an event by event method.

QMD neglects the relativistic part and hence is valid for the incident energies below 1 GeV/nucleon. If one needs to go beyond this energy, one needs to take care of proper relativistic tools. Then one can use relativistic version of QMD i.e. RQMD [43]. Also QMD does not include the isospin effects. Therefore, modified version of QMD, i.e. IQMD has been developed. The present study has been carried out within the framework of IQMD [32] and IQMD (Th01) model [44] and both of these are explained in the following sections.

2.1 Isospin Quantum Molecular Dynamics (IQMD) model

The Isospin Quantum Molecular Dynamics (IQMD) [32] model is an extension of the QMD model which does not incorporate the isospin degree of freedom. In the IQMD model, the isospin degree of freedom enters through the isospin dependent nucleon-nucleon cross-sections, Coulomb interactions, and symmetry potential. The elastic and inelastic cross-sections for proton-proton, neutron-neutron as well as proton-neutron are supposed to be affected in the presence of isospin. In IQMD model, neutron and proton are separated from each other.

The IQMD model treats the different charge states of nucleons, deltas and pions explicitly. The IQMD model has been used successfully for the analysis of large number of observables from low to relativistic energies [45]. This model involve three important steps: First, one has to generate the nuclei. This procedure is called as ***initialization***. The nuclei propagate under the influence of surrounding mean field. This is termed as ***propagation***. Finally, nucleons are bound to collide if they come too close to each other. This part is dubbed as ***collisions***. These three steps are discussed below:

(a) Initialization

Nucleons are represented by Gaussian wave packets which interact by mutual two and three body forces. Each nucleon is represented by a coherent state of the form:

$$f_i(r,p,t) = \frac{1}{\pi^2\hbar^2} e^{-(r-r_i(t))^2\frac{1}{2L}} e^{-(p-p_i(t))^2\frac{2L}{\hbar^2}} \quad (3)$$

where, the Gaussian width (L) represents the interaction range of the particle. The system dependence of L has been introduced in IQMD in order to obtain maximum stability of the nucleonic density profiles. For the heavier system (e.g. Au + Au), its value is chosen to be 8.66 fm^2, while for lighter one (i.e. Ca + Ca), its value is 4.33 fm^2. In order to initialize a nuclei, space and momentum co-ordinates have to be assigned to all the nucleons. In three dimensional space, the centre of Gaussian wave packet r_i are uniformly distributed in polar co-ordinate by

$$r = R\, x_1^{1/3} \quad (4)$$

$$\cos\theta = 1-2x_2 \quad (5)$$

$$\phi = 2\pi x_3 \quad (6)$$

where x_1, x_2, x_3 are the random numbers. The co-ordinates of nucleons are rejected, if the distance between them is less than 1.5 fm. Following the liquid drop model, the nucleons are initialized in a sphere of radius $R=1.12A^{1/3}$ fm. The nucleons are initialized with the momentum, which is randomly chosen between 0 and Fermi momentum (P_F), without any further local constraints in the momentum values. The Fermi momentum P_F depends on the ground state density. For $\rho_0 = 0.17$ fm^{-3}, it has a value of about 268 MeV/c. This possibility, however, gives a reduced binding energy per nucleon as compared to Weizsacker mass formula. Hence, the initialized nuclei are less stable. On the other hand, this situation makes available the full Fermi-energy calculated from the Skyrme ansatz. The full Fermi pressure yields a stronger stability of the density profile against vibrational modes. Moreover, the IQMD model performs a Lorentz contraction of the nucleus coordinate distribution, which becomes important at the higher energies. In order to obtain the smoother distribution of nucleons in phase space, the main requirement is

$$| r_i - r_j |^2 | p_i - p_j |^2 \geq d_{min} \quad (7)$$

Once the target and projectile nuclei are generated with proper initialization, they are boosted with proper center of mass velocity. The propagation is discussed in the next section.

(b) Propagation

The successfully initialized nuclei are then boosted towards each other with proper centre of mass velocity using relativistic kinematics. The centres of projectile and target move along the Coulomb trajectories upto a distance of 2 fm. The interaction between the nucleons of target and projectile through two and three-body Skyrme forces, MDIs and a Yukawa potential. The isospin dependent cross section, symmetry potential and Coulomb interaction explicitly treats the isospin degree of freedom between protons of colliding target and projectile. This gives the correct distribution of protons and neutrons within nucleus.

The propagation of hadrons is explained by using the Hamilton equations of motion:

$$\frac{dr_i}{dt} = \frac{\partial \langle H \rangle}{\partial p_i}; \qquad \frac{dp_i}{dt} = -\frac{\partial \langle H \rangle}{\partial r_i} \tag{8}$$

where,

$$\langle H \rangle = \langle T \rangle + \langle V \rangle$$

$$= \sum_i \frac{p_i^2}{2m} + \sum_i \sum_{j>i} \int f_i(r,p,t) V^{ij}(r',r) \times f_j(r',p',t) dr dr' dp dp' \tag{9}$$

The baryon-baryon potential V^{ij}, in the above relation, reads as:

$$\begin{aligned} V^{ij}(r_i - r_j) &= V^{ij}_{Skyrme} + V^{ij}_{Yukawa} + V^{ij}_{Coul} + V^{ij}_{MDI} + V^{ij}_{sym} \\ &= \left(t_1 \delta(r_i - r_j) + t_2 \delta(r_i - r_j) \rho^{\gamma - 1} \left(\frac{r_i + r_j}{2} \right) \right) + t_3 \frac{\exp(|r_i - r_j|/\mu)}{(|r_i - r_j|/\mu)} + \frac{Z_i Z_j e^2}{|r_i - r_j|} \\ &+ t_4 \ln^2 [t_5 (p_i - p_j)^2 + 1] \delta(r_i - r_j) + t_6 \frac{1}{\rho_0} T_3^i T_3^j \delta(r_i^{'} - r_j) \end{aligned} \tag{10}$$

Here, Z_i and Z_j denote the charges of i^{th} and j^{th} baryon, and T_3^i, T_3^j are their respective T_3 components (i.e. 1/2 for protons and -1/2 for neutrons). The Yukawa term (with t_3= -6.66 MeV and μ=1.5 fm) has been added to improve the surface properties of the interaction which are very important for multifragmentation. Meson potential consists of Coulomb

interaction only. The parameters μ and $t_1 \ldots t_6$ are adjusted to the real part of the nucleonic optical potential [5]

$$V_{loc} = \frac{\alpha}{2}\left(\frac{\rho}{\rho_0}\right) + \frac{\beta}{\gamma+1}\left(\frac{\rho}{\rho_0}\right)^2 \tag{11}$$

Similar to the QMD model, two different EoS have been implemented. A hard nuclear EoS with a compressibility of 380 MeV and a soft EoS with compressibility of 200 MeV [32].

Other baryonic potentials like $V^{ij}_{Skyrme}, V^{ij}_{Yukawa}$ are isospin independent however, the details of MDI and their isospin dependence (IMDI) have been discussed in detail in section 3.1 and 3.2. The model which deals with IMDI i.e. IQMD (Th01) [44] is also discussed in section 3.2. The Yukawa potential V^{ij}_{Yukawa} in IQMD is very short ranged (μ = 0.4 fm in contrast to μ = 1.5 fm in QMD) and weak potential. Yukawa forces stabilize the nuclei because of the increase of the interaction range as compared to a δ-like Skyrme-potential. This results in the reduction of fluctuations. For a nucleus in its ground state, the expectation value of total Hamiltonian corresponds to its total binding energy. On comparing it to the semi empirical mass formula, the Skyrme and MDI contributes to the volume energy and the symmetry interaction contributes to the symmetry energy.

(c) Collision

Although, the collision process is same as in the QMD model, yet the Pauli blocking becomes isospin dependent i.e. the occupancy of phase space of scattering partners is checked for the particles having same isospin as that of the scattered one. In fact , two particles collide if their minimum distance r, i.e. the minimum relative distance of the centroids of the Gaussians during their motion, in their centre of mass frame fulfills the requirement:

$$\left|r_i - r_j\right| \le \sqrt{\frac{\sigma_{tot}}{\pi}}\ , \sigma_{tot} = \sigma\left(\sqrt{s}, type\right) \tag{12}$$

where “type” in above equation denotes the ingoing collision partners (N-N, N-Δ, N – π etc.). In the final state, Pauli blocking is taken into account. The collisions which violate the Pauli principle are neglected.

Whenever a collision occurs, the phase space around the scattering partners is checked. Each nucleon is assumed to occupy a sphere in coordinate and momentum space. This yields the same Pauli blocking ratio as an exact calculation of the overlap of the Gaussians will yield. The fractions P_1 and P_2 of final phase spaces for each of the two scattering partners that is already occupied by other nucleons, is calculated. The collision is blocked with a probability:

$$P_{block} = 1- (1- P_1) (1- P_2) \quad (13)$$

The colliding particles can also scatter elastically or inelastically. At high energies the influence of Pauli blocking is less and kinetic energy is large as compared to the potential. Therefore, total cross section is the sum of elastic and inelastic cross section

$$\sigma_{tot} = \sigma_{el} + \sigma_{inel} = \sigma_{el} + \Sigma_{channels}\sigma_i \quad (14)$$

The next section discusses the various clusterization techniques.

2.2 METHODS OF CLUSTERIZATION:

Once the phase space is generated by the IQMD model, we need to clusterize or group the different particles in the form of fragments according to various conditions. This is done through different clusterization algorithms. These algorithms impose constraints on the relative distance, momentum, or binding energy between two particles and form a fragment accordingly. In this study, we will confine ourselves to only two clusterization techniques/algorithms which are discussed below in brief.

(a) Minimum Spanning Tree (MST):

In MST [29,34,46,54,61] method, two nucleons share the same fragment, if the distance between their centroids are closer than a distance d_{min},

$$|r_i-r_j| \leq d_{min} \quad (15)$$

where, r_i and r_j are the spatial positions of both nucleons. The value of d_{min} can vary between 3-5 fm. This approach allows to define the fragments in a very convenient manner. It is a simplest approach.

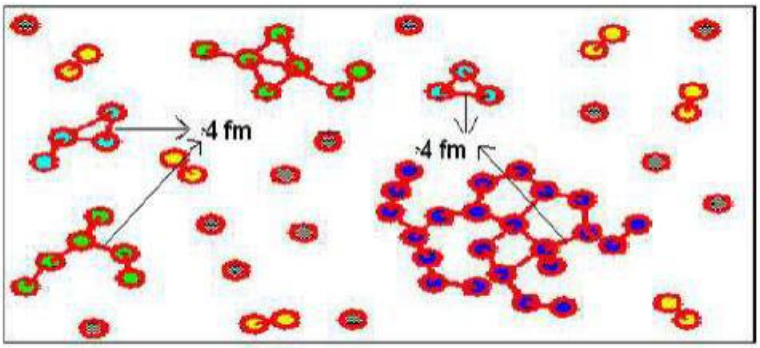

Fig.2.1 : Fragment production using MST method where distance between nucleons is ≤ 4 fm.

(b) Minimum Spanning Tree with Momentum Constraint (MSTP):

As discussed above, the MST method detects the fragments which are close in spatial space only. These fragments may have different momentum. So, MST method does not give the true fragment structure. In order to get the fragments which are close in spatial as well as in momentum space, put an additional constraint on the MST algorithm. This new method with the momentum constraint is known as MSTP [47]. For the true fragmentation, the nucleons required to meet the following conditions:

$$\left|r_i - r_j\right| \leq d_{\min} \tag{16}$$

$$\left|p_i - p_j\right| \leq p_{\min} \tag{17}$$

Where p_{min} of the two nucleons is about the average value of Fermi momentum of nucleons.
In the next chapter, MDI and IMDI are discussed in detail in section 3.1 and 3.2 respectively. In section 3.3, the results and discussions are presented which are based on the analysis of time-scale of fragments with spatial and momentum constraints.

Chapter 3

Effect of isospin momentum dependent interactions on multifragmentation of mass asymmetric colliding nuclei

3.1 Momentum Dependent Interactions (MDI)

The study of intermediate energy HICs need correct treatment of nuclear interactions. MDIs play a very important role in determining the nuclear dynamics. So it is necessary to include the momentum dependent of the mean field generated in HICs [48] to acquire a reasonable theoretical prediction and it is an important feature for the fundamental understanding over a wide range of densities and temperature.

It is widely accepted that the static EoS, which depends only on the density and cannot describe the heavy ion reactions properly. As earlier explained, the contribution in the reaction dynamics is not only due to the density but due to the momentum also. It is argued by many authors that the momentum dependent nature of the EoS can also have a significant effect in those situations where the nuclear matter is mildly and weakly excited. If matter is highly compressed, the nucleon-nucleon correlations are broken due to violent and frequent nucleon-nucleon collisions. If matter is either weakly or mildly excited, the MDI can have sizeable effects. In the framework of G-Matrix, the momentum dependence comes in a natural way [49].

The MDIs can be obtained by parameterizing the momentum dependent part of the optical potential, which is given by [50]

$$V_{MDI}^{ij} = t_4 \ln^2[t_5(p_i^{'} - p)^2 + 1]\delta(r^{'} - r) \tag{18}$$

Here t_4= 1.57 MeV and t_5= 5x10^{-4} MeV^{-2}.

The final form of the momentum dependent potential is given by

$$U = \alpha\left(\frac{\rho}{\rho_0}\right) + \beta\left(\frac{\rho}{\rho_0}\right)^{\gamma} + \delta \ln^2\left[\varepsilon(\Delta p)^2 + 1\right]\frac{\rho}{\rho_0} \tag{19}$$

where γ is the compressibility factor. MDI give rise to the two new EoS, namely Hard momentum dependent (HMD) and soft momentum dependent (SMD), having same compressibility as that of static hard and soft EoS. The MDIs without isospin in IQMD is shown by eq. (18) which comes from optical potential. The initial attempts with MDI have showed a drastic change in the values of collective flow as well as particle production [30,51-53]. The pion yield were found to be suppressed by almost 30% in the presence of MDI [5,29]. MDIs are also found to affect the multifragmentation [54,55] and nuclear stopping [56]. So, MDI play an important role in HICs at intermediate energies.

As discussed earlier, MDI play a crucial role in the description of HICs and can be explained by the Fig. 3.1. We see from the Fig. 3.1 that the momentum of the individual particle has a negligible role until the projectile and target nuclei overlap with each other. As the projectile and target overlapped with each other [see Fig.3.1(a)], the interactions takes place between the nucleons of projectile and target, which has a large relative momentum in

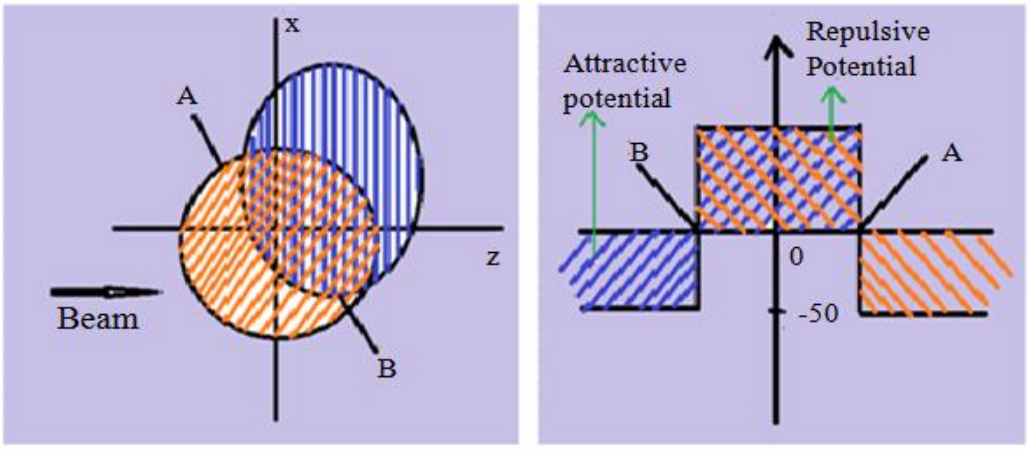

Fig.3.1: Transverse momentum caused by momentum dependent forces. (a) The reaction in the beam-impact parameter plane. (b) Graphical view of the potential produced in the reaction. We see that in the overlap region strong repulsive and outside it an attractive potential. This figure is taken from ref. [29].

comparison to single nuclei. Due to such a large relative momentum, the nucleons of the projectile feels a strong repulsion from the nucleons of the target in the overlapped region and vice-versa. [see Fig.3.1(b)], while the nucleons in the spectator zone are either from the projectile or from the target and hence potential is still attractive in the spectator region [see Fig. 3.1(b)] and in this region mean field dominates. This deflects the nucleons in the transverse direction during the early phase of the reaction, which results in the transfer of

momentum in the radial direction. Hence results in decrease in density as well as number of collisions. The isospin dependence of MDI have been discussed in detail in the next section.

3.2 Isospin Momentum Dependent Interactions (IMDI)

Although the role of MDI in the reaction dynamics in HICs has been investigated from many years, but the effect of IMDI have not gain much importance. Liu *et al.* [57] for the first time, considered an isospin degree of freedom into the MDI to obtain IMDI which should be different for neutrons and protons. To study the effect of IMDI on the reaction dynamics of HICs, they put an isospin degree of freedom in the MDI in IQMD to obtain the IMDI. It has been found that IMDI induces the significant reduction in the isospin fractionation ratio [58]. Therefore, the isospin factor of the MDI is important for extracting the information about the EoS of asymmetrical nuclear matter.

The methodology for the isospin term, which uses in the MDI to obtain IMDI is based on the fact that neutron-proton correlations are stronger than the neutron-neutron, proton-proton correlations [59,60]. Then the isospin based MDI potential can be read as

$$V_{IMDI}^{ij} = \left(1.0 - 0.5T_3^i T_3^j\right) V_{MDI}^{ij} \tag{20}$$

Where T_3^i and T_3^j are the isospin components of interacting baryons. This new model with inclusion of isospin into the MDI is known as IQMD (Th01) model [44]. Such that the total potential in IQMD (Th01) takes the form:

$$V = V_{Skyrme} + V_{Yukawa} + V_{Coul} + V_{IMDI} + V_{sym} \tag{21}$$

The compressional energy per particle for static (soft and hard EoS) and momentum-dependent interactions (SMD and HMD EoS) as a function of density is shown in Fig.1.6. From the figure, it is clear that there is no difference between static and momentum-dependent EoS at normal nuclear matter density. However, the difference between different EoS goes on increasing with the increase in density above normal nuclear matter density. Thus, the MDIs govern the dynamics of HICs. These results motivated us to study IMDI in intermediate energy HICs.

Lots of studies have been reported in the literature that focuses the effect of MDI on multifragmentation [54,55]. These studies predicted a significant effect of MDI on multifragmentation at peripheral collisions [61]. Unfortunately, no study has been carried out to look into the details of the fragment structure using IMDI. However, many authors have studied the role of IMDI and proposed an important spin effect into the isospin fractionation ratio (IsoFR) and the dynamical mechanism involved in the intermediate energy HICs [57,62]. Jun Xu *et. al.* [63] gives IMDI in-medium effective interactions for the baryon octet, which will be useful in transport models that simulate HICs in future radioactive beam facilities, particularly at *FAIR/GSI* energies. Within the framework of IBUU transport model, an extensive amount of work has been carried out to study the various isospin-sensitive observables using IMDI in intermediate energy HICs [1,64]. Also, Das Gupta and others gave a formula for IMDI and Skyrme potential for Boltzmann-Uhling-Uhlenbeck (BUU) calculations and for HICs induced by neutron-rich nuclei [65]. From the above review, it is clear that the role of IMDI in the multifragmentation of asymmetric colliding nuclei will be interesting to be investigated. The results related to the work carried out for the present objective are discussed in the next section.

3.3 RESULTS and DISCUSSION

In the previous chapter, the details of heavy ion reactions and the different methods to deal with them have been discussed in detail. For the detailed investigation of IMDI in the asymmetric reactions, the simulations have been carried out for various mass asymmetric systems namely ${}^{12}_{6}C+{}^{197}_{79}Au$ (η=0.8), ${}^{24}_{12}Mg+{}^{197}_{79}Au$ (η=0.7), ${}^{40}_{18}Ar+{}^{197}_{79}Au$ (η=0.6), ${}^{56}_{26}Fe+{}^{197}_{79}Au$ (η=0.5), ${}^{83}_{36}Kr+{}^{197}_{79}Au$ (η=0.4) and ${}^{131}_{54}Xe+{}^{197}_{79}Au$ (η=0.2) for the full range of incident energy (40 to 600 MeV/nucleon) and scaled impact parameter, $\hat{b} = b/b_{\max} = 0, 0.3, 0.6, 0.9$ [where b is particular impact parameter in Fermi (fm) and $b_{max} = 1.12(A_T^{1/3} + A_P^{1/3})$, A_T and A_P are the masses of target and projectile nuclei respectively]. Since b_{max} is different for different systems, hence the value of $\hat{b}$ will obviously be different for different systems. In addition to these, the reactions of ${}^{40}_{20}Ca+{}^{197}_{79}Au$ (N/Z=1), ${}^{48}_{20}Ca+{}^{197}_{79}Au$ (N/Z=1.4), ${}^{52}_{20}Ca+{}^{197}_{79}Au$ (N/Z=1.6), ${}^{60}_{20}Ca+{}^{197}_{79}Au$ (N/Z=2.0) have also been studied. A soft EoS has been employed with momentum dependent interactions named SMD and with isospin momentum dependent interactions named as ISMD. Motivated by the extensive study carried out by K.S. Vinayak

[66], the form of the density dependent symmetry energy corresponding to $\gamma = 0.66$ has been chosen. The reaction has been carried out till 200 fm/c, which is considered as saturation time. The phase space produced by the IQMD and IQMD (Th01) models have been analyzed with MSTP technique, in which d_{min} is chosen to be 4 fm and p_{min} is chosen to be 150 MeV/c.

3.4 Snap shot of the Phase Space

3.4.1 Spatial and momentum Distribution

A plot of position and momentum co-ordinates as a function of time is sometimes known as phase plot or phase diagram. Fig.3.2 and 3.3 shows the phase space of projectile and target nucleons in X-Z and P_x-P_z plane for the mass asymmetric reactions namely ${}^{12}_{6}C+{}^{197}_{79}Au$, ${}^{56}_{26}Fe+{}^{197}_{79}Au$, ${}^{131}_{54}Xe+{}^{197}_{79}Au$ for $\hat{b}=0.3$ and $E=100\,MeV/nucleon$.

As a first step, the phase space distribution of the projectile and target nucleons have been visualized. The panels from top to bottom represents the results at different time steps.

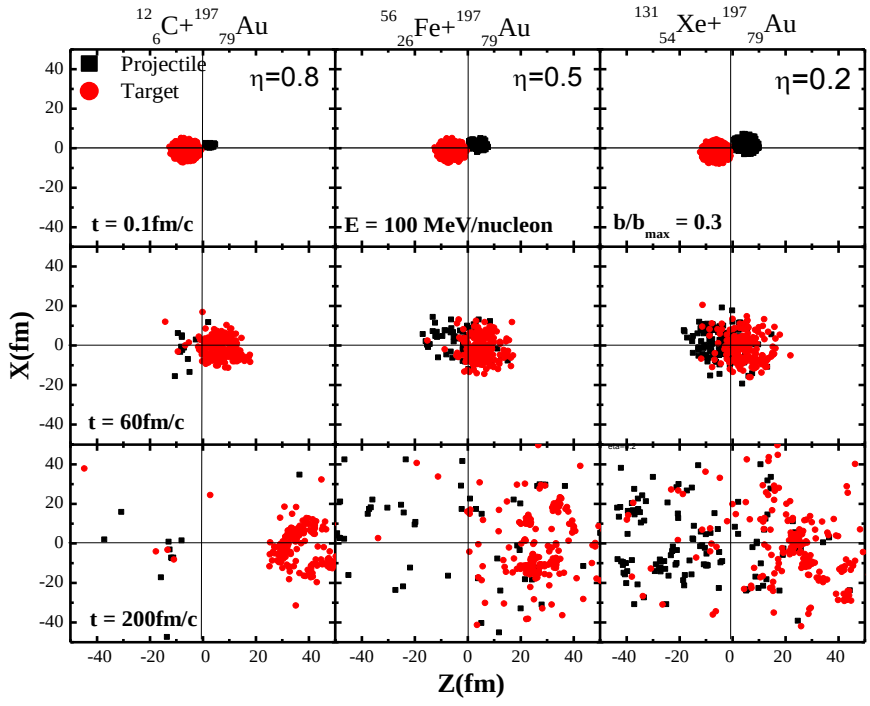

Fig.3.2: Coordinate space distribution of the projectile and target nucleons in X-Z plane. The reactions under study are ${}^{12}_{6}C+{}^{197}_{79}Au$, ${}^{56}_{26}Fe+{}^{197}_{79}Au$ ***and*** ${}^{131}_{54}Xe+{}^{197}_{79}Au$ ***at an incident energy E=100 MeV/nucleon and scaled impact parameter,*** $\hat{b}=0.3$***. The panels from top to bottom are representing the coordinate space of nucleons at different times.***

We display the coordinate and momentum space distribution of the nucleons of projectile and target for the reactions having mass asymmetry η= 0.8, η=0.5 and η=0.2. After the overlapping stage, repulsion is generated for projectile as well as target nucleons. While the projectile nucleons travel through the target and they experience the strong transverse thrust due to strong density gradient at the surface of the projectile. We note that for nearly symmetric collisions having η=0.2 (in the right panel) lead to a spherical distribution, while for the highly asymmetric collisions having η=0.8 (in the left panel) lead to a non-spherical distribution for both the co-ordinate and momentum phase space distribution. This is due to the reason that number of nucleons in projectile and target are different in both cases. Therefore, the contribution of the participant and spectator matter will also be different for all the reactions. Thus, the contribution of the mean-field and NN collisions will also different for different systems.

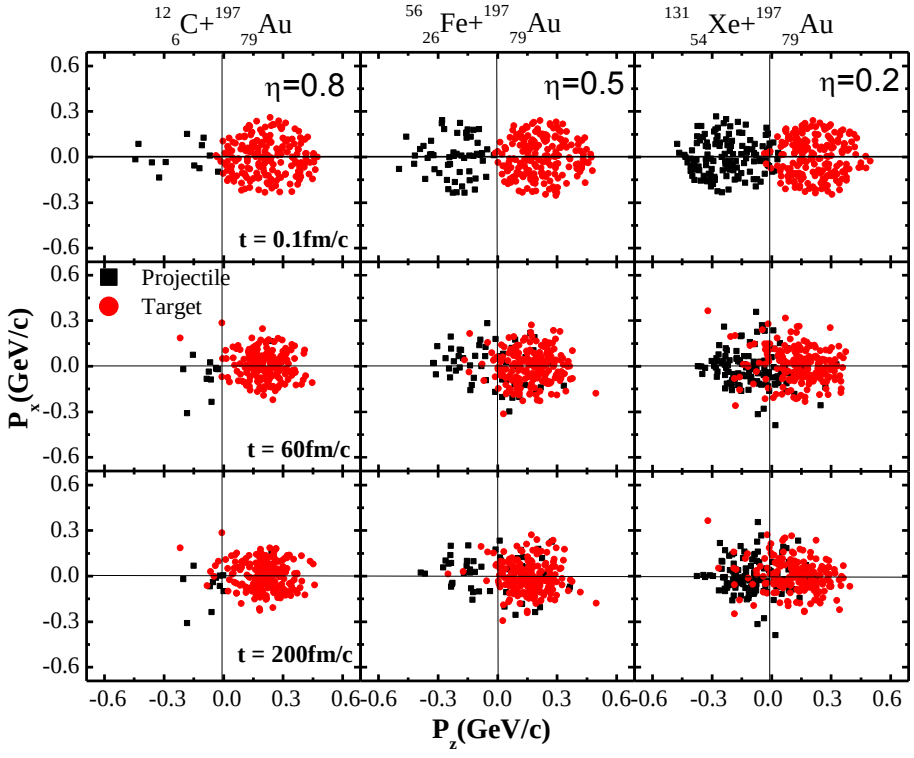

Fig.3.3: Same as in Fig.3.2, but for the momentum distribution of the nucleons in P_x-P_z plane.

Fig.3.4 and 3.5 shows the same distribution in X-Z and P_x-P_z plane for the reverse reactions as has been shown in the last section. Here the gold nuclei has been taken as projectile and targets are ${}^{12}_{6}C$, ${}^{56}_{26}Fe$, *and* ${}^{131}_{54}Xe$.

In figures 3.4 and 3.5, the trends are just opposite as that from the previous results.

3.4.2 Variation of maximum density $\left(\langle \rho/\rho_0 \rangle^{max}\right)$ and average density $\left(\langle \rho/\rho_0 \rangle^{avg}\right)$ with time

When the nuclear matter is subjected to high compression, the large density built up during the reaction will be different for different colliding nuclei. In such a case, it will be interesting to study the nuclear dynamics for the different projectiles and same target nuclei. To investigate the behaviour of density, an approach mentioned in [67] has been applied.

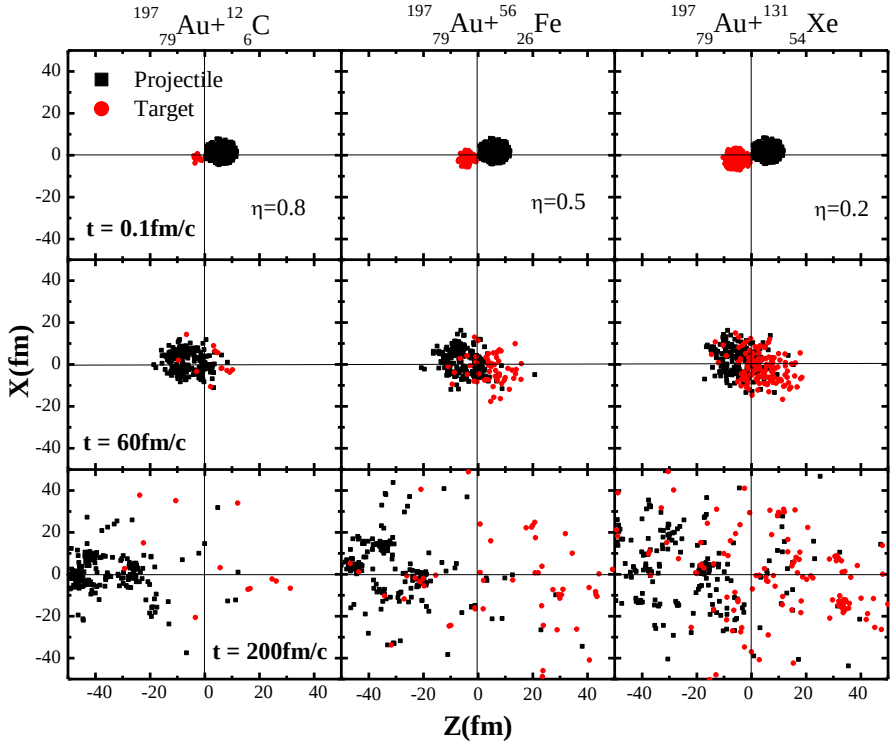

Fig.3.4: Same as Fig.3.2, but for the reversed reactions.

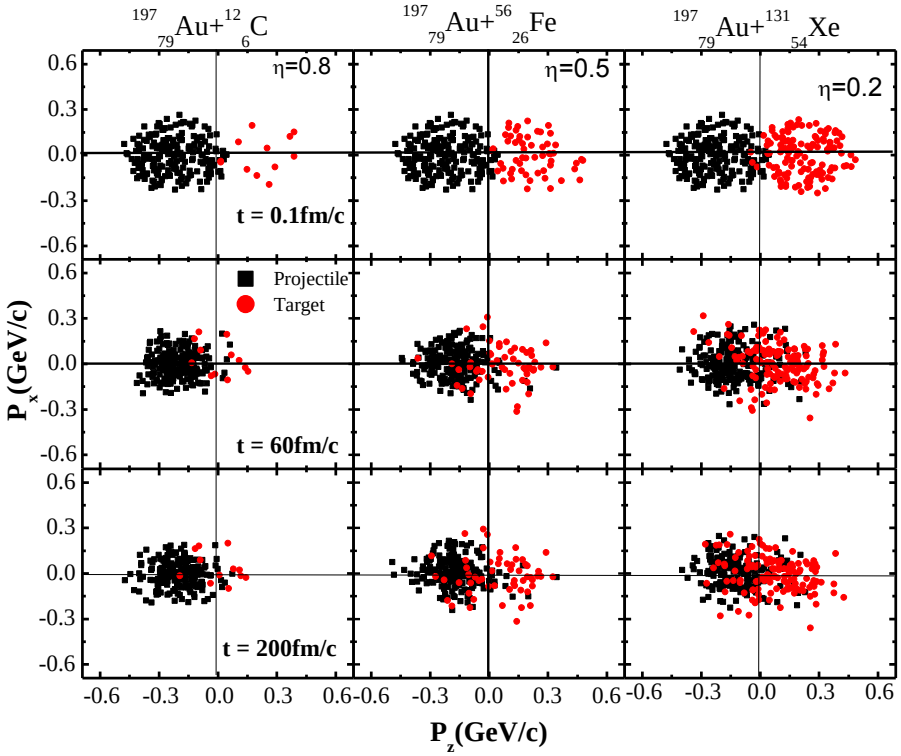

Fig.3.5: Same as Fig.3.4, but for the P_x-P_z plane.

According to this, the density can be defined as:

$$\rho(r,t) = \sum_{i=1}^{A_T+A_P} \frac{1}{2\pi L}.\exp\left[-(r-r_i(t))^2/2L\right] \qquad (22)$$

Here, L is the Gaussian width of the wave packet. The above density is calculated in the central sphere of radius 2 fm. This procedure of density determination leads us to two possibilities: either (i) one can look for the maximum density $\left(\langle\rho/\rho_0\rangle^{max}\right)$ reached anywhere in this sphere or (ii) one can take an average value over the whole sphere $\langle\rho/\rho_0\rangle^{avg}$.

In Fig.3.6, the time evolution of the $\langle\rho/\rho_0\rangle^{max}$ for the different mass asymmetric reactions at an incident energy of 100 MeV/nucleon and $\hat{b}=0.3$ under the influence of SMD (in upper panel) and ISMD (in lower panel) has been displayed. From the figure, it is clear that, with the increase in time, the $\langle\rho/\rho_0\rangle^{max}$ first increases and then decreases for all the asymmetric reactions. Rise and fall with time is observed in the behaviour of maximum density. The $\langle\rho/\rho_0\rangle^{max}$ with SMD and ISMD shows the same trend. This is because initially, the nuclei

are overlapping and highly compressed which gives the highly dense phase of nuclear matter. With the passage of time, when nucleon-nucleon collisions occurred and then over, at that time, there is a saturation in the collisions and hence in the nuclear matter density also. With decrease in the size of the projectile, the $\langle \rho/\rho_0 \rangle^{max}$ for both SMD and ISMD decreases, because due to the smaller size of the projectile, the participant zone is less, so the compression achieved is also less, which leads to the lower $\langle \rho/\rho_0 \rangle^{max}$. The peak value of $\langle \rho/\rho_0 \rangle^{max}$ shifts towards the higher time for heavier mass projectiles, because due to the large number of participating nucleons, the colliding nuclei takes more time to completely compress each other.

Similar to Fig.3.6, in Fig.3.7, the dependence of $\langle \rho/\rho_0 \rangle^{avg}$ on time has been displayed. It is clear from the figure, that the $\langle \rho/\rho_0 \rangle^{avg}$ shows the same behaviour (i.e. rise and fall) as that of $\langle \rho/\rho_0 \rangle^{max}$. Also, the uniform distribution of the nucleons in the dense nuclear matter leads to almost similar values of $\langle \rho/\rho_0 \rangle^{max}$ and $\langle \rho/\rho_0 \rangle^{avg}$.

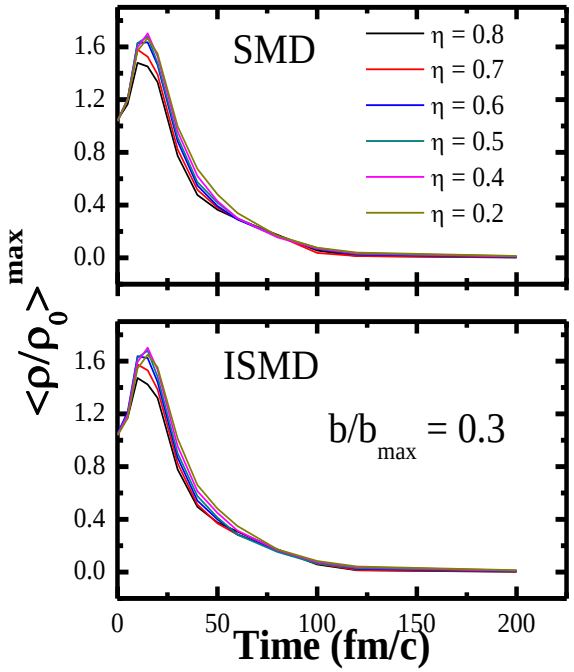

Fig.3.6: The variation of maximum density $\left(\langle \rho/\rho_0 \rangle^{max}\right)$ ***with time at the incident energy of 100 MeV/nucleon and*** $\hat{b} = 0.3$***. Different lines represent the results for different mass asymmetries. The upper and lower panels are for SMD and ISMD respectively.***

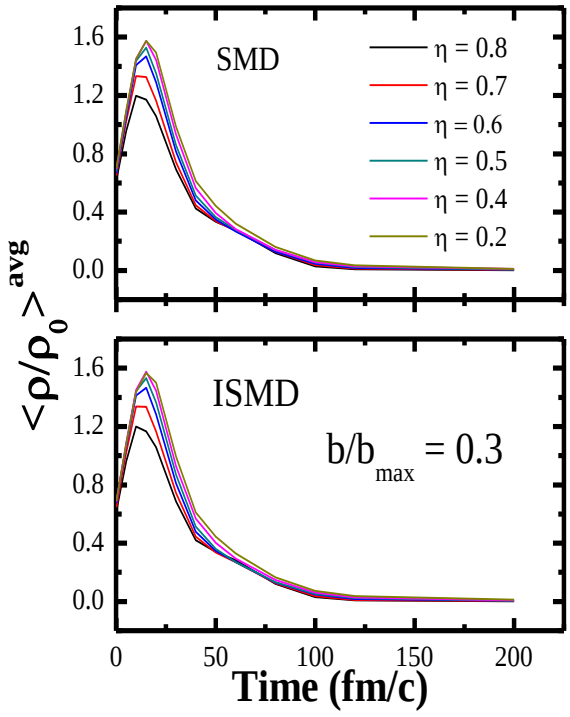

Fig.3.7: Same as Fig.3.6, but for average density $\left(\langle \rho / \rho_0 \rangle^{avg}\right)$.

3.4.3 Dependence of the allowed collision rate $\left(\langle dN_{coll} / dt \rangle^{allowed}\right)$ on time

Fig.3.8 shows the allowed collision rate $\left(\langle dN_{coll} / dt \rangle^{allowed}\right)$ as a function of time for the different mass asymmetric reactions at an incident energy of 100 MeV/nucleon and $\hat{b} = 0.3$. The upper panel shows the results for SMD while lower panel shows the results for ISMD. The figure depicts that, with the passage of time, the collision rate first decreases from time step 0.1 fm/c and then increases upto 15 fm/c. After that the collision rate decreases and then it saturates at time 200 fm/c and this trend is followed by all the reactions. But for the nearly symmetric reaction, collision rate increases till time 20 fm/c and then decreases. This is due to the reason that with the passage of time, compression in the nuclear matter decreases, which gives the lesser density that leads to the decrease in the collision rate with time for both SMD as well as ISMD. The allowed collision rate is not varied much by the ISMD. Also for the reaction with heavier projectile, the allowed collision rate is larger as compared to the reaction with lighter projectile. This is caused due to the increase in the participant matter, which leads to larger nucleon-nucleon collisions.

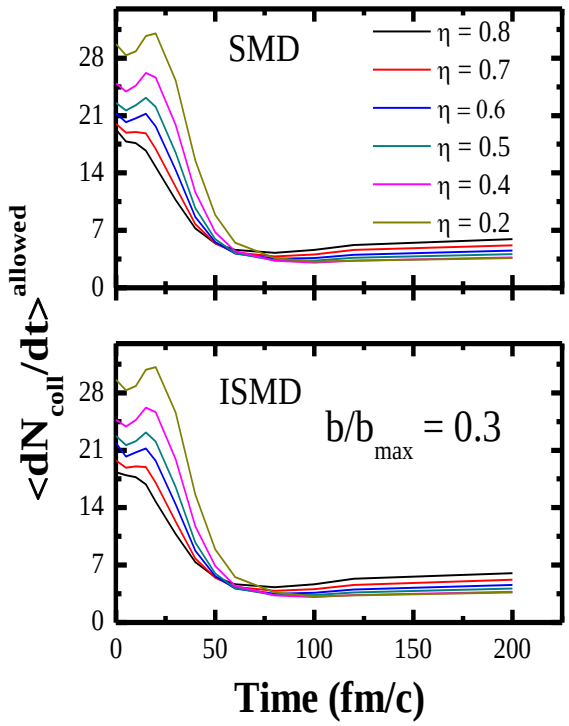

Fig.3.8: The variation of the allowed collision $\left(\langle dN_{coll}/dt\rangle^{allowed}\right)$ ***rate with time at an incident energy of 100 MeV/nucleon and*** $\hat{b}=0.3$ ***under the influence of SMD (shown in upper panel) and ISMD (shown in lower panel). Different lines represent the results for different mass asymmetries.***

3.4.4 Time evolution of various fragments

In Fig.3.9, the time evolution of the multiplicity of different fragments has been displayed for the reactions ${}^{12}_{6}C+{}^{197}_{79}Au$ and ${}^{131}_{54}Xe+{}^{197}_{79}Xe$ with η = 0.8 (highly asymmetric) and 0.2 (nearly symmetric) respectively at an incident energy of 100 MeV/nucleon and $\hat{b}=0.3$ under the influence of SMD and ISMD. The panels from top to bottom shows the multiplicity of different fragments such as free nucleons [FNs (A=1)], light mass fragments [LMFs (2≤A≤4)] and intermediate mass fragments [IMFs(5≤A≤$A_{tot/6}$)], while the left and right panels show the different reactions for which the multiplicity has been calculated.

With the passage of time, the multiplicity of various fragments increases for both SMD as well as ISMD. In the ${}^{12}_{6}C+{}^{197}_{79}Au$ reaction, the projectile nuclei is lighter as compared to the projectile of the ${}^{131}_{54}Xe+{}^{197}_{79}Au$ reaction. For the case of ${}^{12}_{6}C+{}^{197}_{79}Au$, the values of multiplicities for FNs, LMFs, and IMFs produced with SMD are larger than that for with ISMD. Because

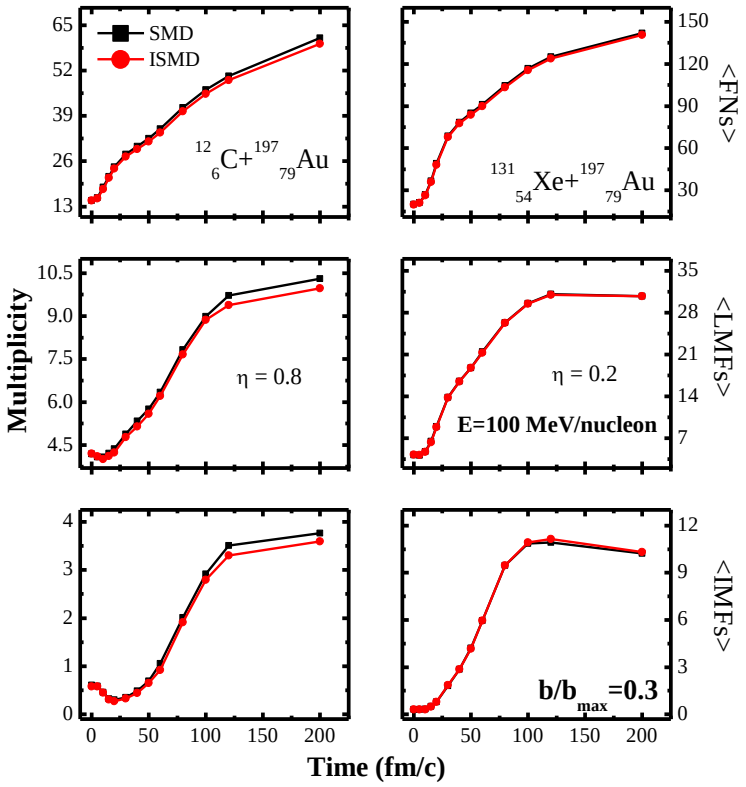

Fig.3.9: The time evolution of the multiplicity of FNs (A=1), LMFs (2≤A≤4) and IMFs (5≤A≤$A_{tot/6}$) for two different reactions, in which one is highly asymmetric (shown in the left panel) and the other is nearly symmetric (shown in the right panel) at an incident energy of 100 MeV/nucleon and $\hat{b} = 0.3$**.**

in case of SMD, the repulsion among all the nucleons are equal while for the ISMD, the repulsion among the neutron-proton pair is lesser as compared to neutron-neutron and proton-proton. Due to the larger repulsion with SMD, the shattering of the matter into FNs, LMFs and IMFs is also large. Also, due to the larger participant matter in case of $^{131}_{54}Xe+^{197}_{79}Au$, the number of emitted FNs, LMFs and IMFs are greater. Whereas, the larger spectator matter gives rise to the heavier fragments in case of lighter projectile reaction. It is found that for the lighter projectile reaction, the SMD as well as ISMD shows the difference in the multiplicity values whereas, for heavier projectile reaction, there is no difference between SMD and ISMD because in the former case, the spectator part is more and the SMD plays a significant role in the spectator part, so for the ISMD and hence the result follows. From this figure, it can be concluded that, ISMD plays a significant role for the lighter projectile reaction, so for the further investigation, the results are displayed only for the reaction $^{12}_{6}C+^{197}_{79}Au$.

3.4.5 Energy dependence of the multiplicity of various fragments

Fig.3.10, shows the energy dependence of the total multiplicity for the lighter projectile case i.e. ${}^{12}_{6}C+{}^{197}_{79}Au$ at $\hat{b}=0.3$ under the influence of SMD and ISMD. The figure shows that the multiplicity of FNs, LMFs and IMFs increases with the increase in incident energy because with the increase in energy, the compression increases and more matter is driven into the participant zone due to which the correlations between the particles break and hence the multiplicity of various fragments increases.

It is to be noted here that the multiplicity of IMFs keeps on increasing with the incident energy because for the ${}^{12}_{6}C+{}^{197}_{79}Au$, the spectator zone is larger and the role of SMD is more violent in this region which breaks the heavier fragments into more IMFs. The ISMD plays a

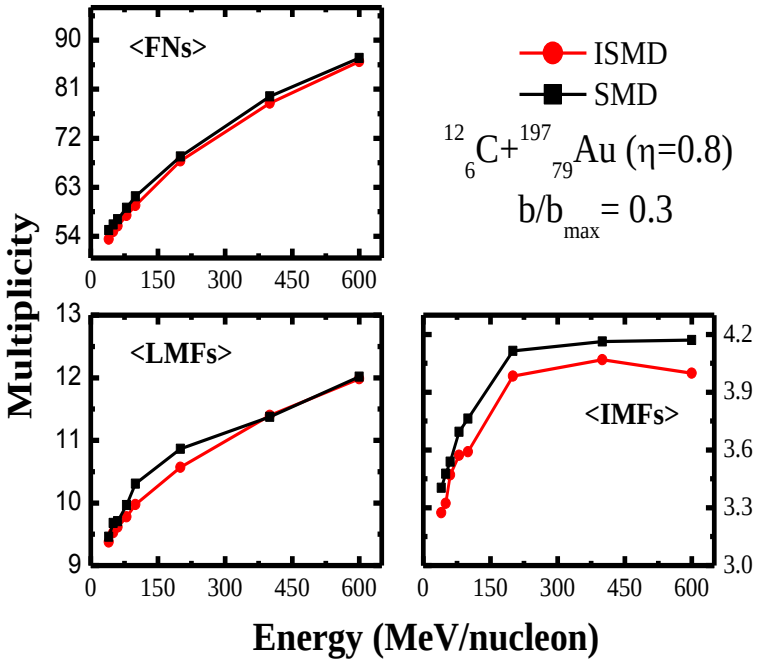

Fig.3.10: Dependence of the multiplicity of various fragments with energy at $\hat{b}=0.3$ ***for*** ${}^{12}_{6}C+{}^{197}_{79}Au$ ***under the influence of SMD (shown by line with square symbols) and ISMD (shown by line with circle symbols).***

significant role for the IMFs at all the incident energies, whereas the FNs and LMFs are slightly sensitive towards the ISMD. The multiplicities of FNs and IMFs are larger with SMD as compared to ISMD for all the incident energies, because of more repulsive nature of the

SMD as compares ISMD, the shattering of matter is more and hence the result follows. The above scenario is also observed for LMFs, but upto 400 MeV/nucleon. After that SMD and ISMD gives the same results.

3.4.6 Impact parameter dependence of the multiplicity of various fragments

Fig.3.11 displays the multiplicities of various fragments (FNs, LMFs, IMFs) as a function of the scaled impact parameter for the lighter projectile reaction named ${}^{12}_{6}C+{}^{197}_{79}Au$. From the figure, it is clear that the multiplicity of the various fragments decreases with the increase in the impact parameter. It is because of the fact that with the increase in the impact parameter, participant zone decreases and the spectator zone increases. With the increase in the spectator

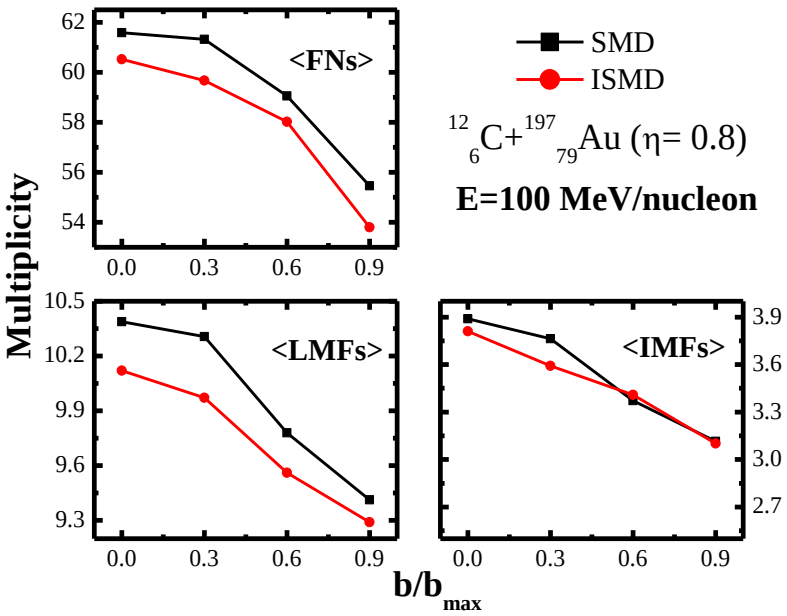

Fig.3.11: Dependence of the multiplicity of different fragments (FNs, LMFs and IMFs) on the scaled impact parameter for the reaction with η=0.8 at an incident energy of 100 MeV/nucleon. Lines with square and circle symbols displays the results for SMD and ISMD respectively.

zone, most of the nucleons in the spectator part goes unreacted and hence very large fragments are produced which goes out of the range of IMFs also. Therefore, with the increase in the impact parameter, the multiplicity of the various fragments decreases for the

$^{12}_{6}C+^{197}_{79}Au$ reaction. Also, we see the difference between SMD and ISMD because of the reason that for η=0.8, spectator part is larger in which the SMD and ISMD plays a significant role. The multiplicities of FNs, LMFs and IMFs are larger in case of SMD as compared to ISMD, because the SMD is equally repulsive for all the nucleons, whereas, ISMD is more repulsive for neutron-neutron and proton-proton as compared to the neutron-proton. This larger repulsion generated in case of SMD gives rise to more shattering of the matter.

3.4.7 Energy and Impact parameter dependence of the largest fragment $\left(\left\langle A^{\max}\right\rangle\right)$

For the further investigation, the influence of ISMD with respect to SMD has been investigated with the help of maximum mass fragment $\left(\left\langle A^{\max}\right\rangle\right)$ over the different incident

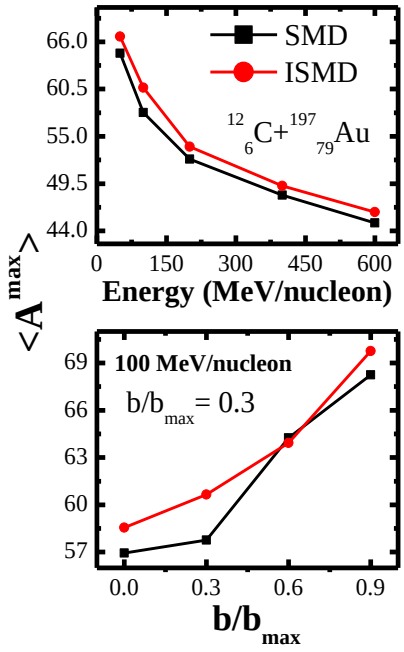

Fig.3.12: The variation of the largest fragment $\left\langle A^{\max}\right\rangle$ ***with energy at impact parameter*** $\hat{b}=0.3$ ***shown by the upper panel, while the lower panel shows the variation of*** $\left\langle A^{\max}\right\rangle$ ***with impact parameter at an incident energy 100 MeV/nucleon for asymmetric (left panel) and nearly symmetric (right panel) reactions.***

energies (in the upper panel) and whole colliding geometry (in the lower panel). This investigation has been made for the lighter projectile reaction i.e. for η=0.8. From the figure,

it is clear that, with increase in the incident energy, the $\langle A^{max} \rangle$ decreases for SMD as well as ISMD because with the increase in energy, the correlations between the particles break. As a result of this, $\langle A^{max} \rangle$ decays into lighter fragments and free nucleons.

The role of ISMD is influential for η=0.8 because in this case, more matter is driven into the spectator part, which contribute towards the higher $\langle A^{max} \rangle$, and as we know that in the spectator part, role of SMD is significant, so with the case of ISMD. Also, the $\langle A^{max} \rangle$ is larger with ISMD, because ISMD is lesser repulsive as compared to the SMD, which keeps the nucleons together and hence the result follows.

On the contrary, with increase in the impact parameter, the $\langle A^{max} \rangle$ increases, due to the increase in the spectator part. Here also, ISMD influences the $\langle A^{max} \rangle$ significantly.

3.4.8 Variation of the bound charged fragment $(\langle Z_{bound} \rangle)$ with Energy and Impact parameter

One more expected probe for ISMD is the bound charged fragment $(\langle Z_{bound} \rangle)$. **$Z_{bound}$** is defined as the sum of the atomic numbers Z_i of all the fragments with $Z_i \geq 2$.

In Fig.3.13, the variation of the $\langle Z_{bound} \rangle$ is shown with the incident energy (in the upper panel) and over the whole colliding geometry (in the lower panel) for η=0.8. The figure depicts that with the increase in incident energy, $\langle Z_{bound} \rangle$ decreases for both the interactions (SMD and ISMD). This is because, the higher incident energy gives rise to more breakage of the initial correlations among the nucleons, which prevent the charged particles to remain together. On the contrary, from the lower panels, it is clear that $\langle Z_{bound} \rangle$ increases with the increase in the impact parameter, because with increase in the impact parameter, spectator part is larger, in which most of the initial correlations are not broken, which helps to keep the charged fragments together, hence the result follows.

There is a significant effect of ISMD in the ${}^{12}_{6}C+{}^{197}_{79}Au$ reaction. The $\langle Z_{bound} \rangle$ formed with the SMD is smaller as compared to that with ISMD, because for ISMD, neutron-proton correlations are stronger as compared to neutron-neutron and proton-proton, which leads less breaking of the initial correlations as compared to the SMD which is equally repulsive for all

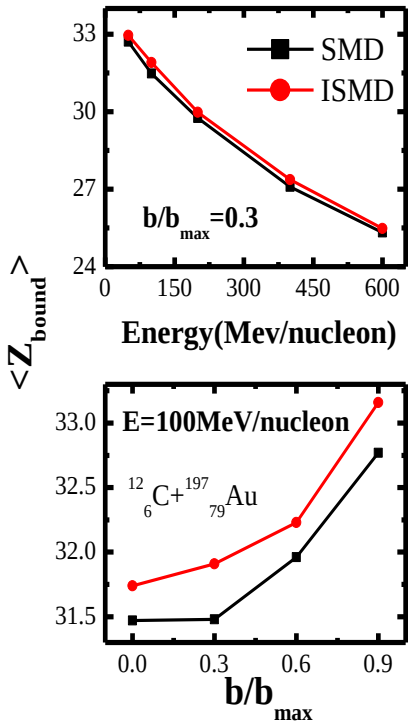

Fig.3.13: Same as Fig.3.12, but for $\langle Z_{bound} \rangle$.

the nucleons. This larger repulsion in case of SMD keeps the charged particles far apart and hence lesser value of $\langle Z_{bound} \rangle$ with SMD as compared to ISMD.

3.4.9 Single neutron to proton ratio ($R_{N/Z}$)

The single ratio is just the ratio of neutrons to protons. It is represented by $R_{N/Z}$ in the present study. Various experimental and theoretical studies have been reported in the literature that focuses on the single ratio of neutron to proton. Some of these are mentioned in the following paragraph.

D. Polster *et al.* [68] studied the $R_{N/Z}$ for the thirteen targets in the mass range of A= 12 – 238 at the low energy antiproton ring (LEAR) at CERN, Geneva. They observed that $R_{N/Z}$ of directly emitted neutrons to protons have been determined about twice the $R_{N/Z}$ in the target nucleus nearly independent of its mass. M. Dzelalija *et al.* [69] also studied the $R_{N/Z}$ for the data of Au+Au central reaction between 100 MeV/nucleon and 400 MeV/nucleon at the GSI using the 4π detector system named FOPI. Their analysis has allowed for the extraction of the baryonic density, temperature and flow. Another experiment was performed at GANIL facility and the charge products were detected with INDRA multidetector. N. Marie *et al.* [70] studied the reaction of $^{129}Xe+^{nat}Sn$ for central colliding geometry at 50 MeV/nucleon. Their study indicates that the primary excited fragments have the same $R_{N/Z}$ as that of the

initial system Xe+Sn. Another experiment [8] in which the N/Z dependence of projectile fragmentation at the incident energy of 600 MeV/nucleon has been studied with the ALADIN forward spectrometer at the GSI Schwerionen Synchrotron (SIS). They showed that fragmentation observables depend weakly on the projectile N/Z ratio, while substantial differences are observed for the light fragments ($Z \leq 10$). M. Colonna *et al.* [71] studied the effect of $(N/Z)_{liq\text{-}gas}$ at Fermi energies for the neutron rich and symmetric systems as a function of the initial $(N/Z)_{in}$. They observe that the gas phase is generally more neutron rich than the liquid phase and the liquid phase is more symmetric. X.Y. Sun *et al.* [72] studied the dependence between $R_{N/Z}$ and neutron skin thickness (δ_{np}) in neutron rich nuclei $^{50}Ca+^{12}C$ at 50 MeV/nucleon within the framework of IQMD model. They observed a good linear correlation between $R_{N/Z}$ and δ_{np} for neutron rich projectile. Their work suggest that $R_{N/Z}$ could be used as an experimental tool to extract the δ_{np} for neutron rich nucleus. $R_{N/Z}$ is very important tool to study the EoS of asymmetric nuclear matter. J. Xu *et al.* [73] studied the dependence of $R_{N/Z}$ on the symmetry energy for U+U collision at 0.52 GeV/nucleon using an isospin and momentum dependent interactions within the framework of the IBUU model and concludes that the $R_{N/Z}$ of pre-equilibrium nucleons are slightly more sensitive to the symmetry energy.

In our above studies, the multiplicities of various fragments have been analyzed under the influence of ISMD and it is concluded that ISMD plays a significant role for the lighter projectile reaction. Now, for the further investigation, it will be interesting to check the effect of ISMD on the constituents of various fragments.

(i) Dependence on incident energy

In Fig. 3.14, the dependence of $R_{N/Z}$ on the incident energy has been tested for the various fragments (FNs, LMFs, IMFs) under the effect of SMD (shown by black lines) and ISMD (shown by red lines). This analysis has been made for two reactions: lighter projectile reaction ($^{12}_{6}C+^{197}_{79}Au$) and heavier projectile reaction ($^{131}_{54}Xe+^{197}_{79}Au$). The figure leads to the following conclusions:

a) The $R_{N/Z}$ decreases with increase in the incident energy for both the reactions as well as for the two interactions. For the case of FNs, this may be due to the reason that at 600 MeV/nucleon, there is production of pions also. Also, as the incident energy increases, more and more protons become unbound as compared to neutrons, which thereby decreases the $R_{N/Z}$ for FNs.

b) The values of $R_{N/Z}$ for LMFs and IMFs are larger for ISMD compared to SMD over the entire energy regime, whereas the opposite trend is there for the FNs which means that the gas phase is more enriched with neutrons for SMD, therefore the $R_{N/Z}$ having a larger value for SMD for FNs , whereas, the liquid phase is more enriched with neutrons for ISMD, therefore the $R_{N/Z}$ having a larger value for ISMD for LMFs and IMFs. This is due to the more repulsive nature of SMD in comparison to ISMD.

c) Also, the $R_{N/Z}$ for lighter projectile reaction is more affected by the ISMD as compared to the heavier projectile reaction.

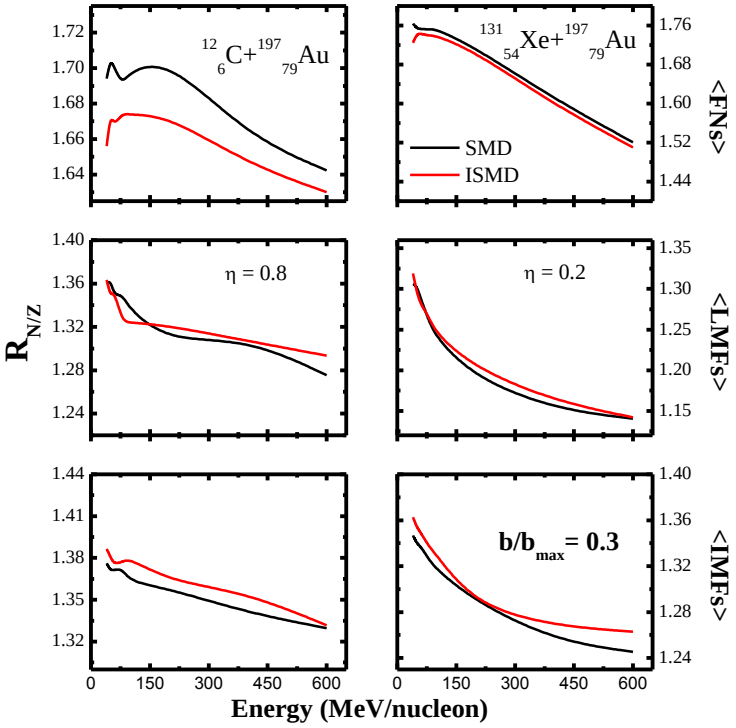

Fig.3.14: Variation of the single neutron to proton ratio ($R_{N/Z}$) with the incident energy for various classes of fragments under the influence of SMD (shown by black lines) and ISMD (shown by red lines).

ii) Variation of the multiplicity and $R_{N/Z}$ on the projectile neutron-proton ratio $(N/Z)_{Proj.}$

Lastly, the multiplicity and $R_{N/Z}$ has been simultaneously tested for the reactions of different isotopic projectiles of Ca on the Au target. For this, Fig.3.15 shows the multiplicity (left panel) and $R_{N/Z}$ (right panel) with the neutron-proton ratio of the projectile $(N/Z)_{Proj.}$. This analysis has been performed at an incident energy 100 MeV/nucleon and $\hat{b} = 0.3$ under the

influence of SMD (shown by black lines) and ISMD (shown by red lines). The figure reveals the following important conclusions:

a) With increase in the $(N/Z)_{Proj.}$, multiplicity of all the fragments (FNs, LMFs, IMFs) increases, which is obviously due to the increase in the participating nucleons. The $R_{N/Z}$ also shows an increasing behaviour with the $(N/Z)_{Proj.}$. This is due to the increase in the number of neutrons in the whole system.

b) The multiplicity of FNs and LMFs is larger with the SMD for all the $(N/Z)_{Proj.}$ which is caused by the more repulsive nature of SMD compared to ISMD. Corresponding to this, the $R_{N/Z}$ is larger with SMD for FNs, while, it is larger for IMFs with ISMD. This is because of the reason that SMD drives more neutrons into the gas phase in comparison to ISMD, whereas, ISMD drives more protons into the liquid phase as compared to SMD.

Part of these results has been shown in ref. [74,75].

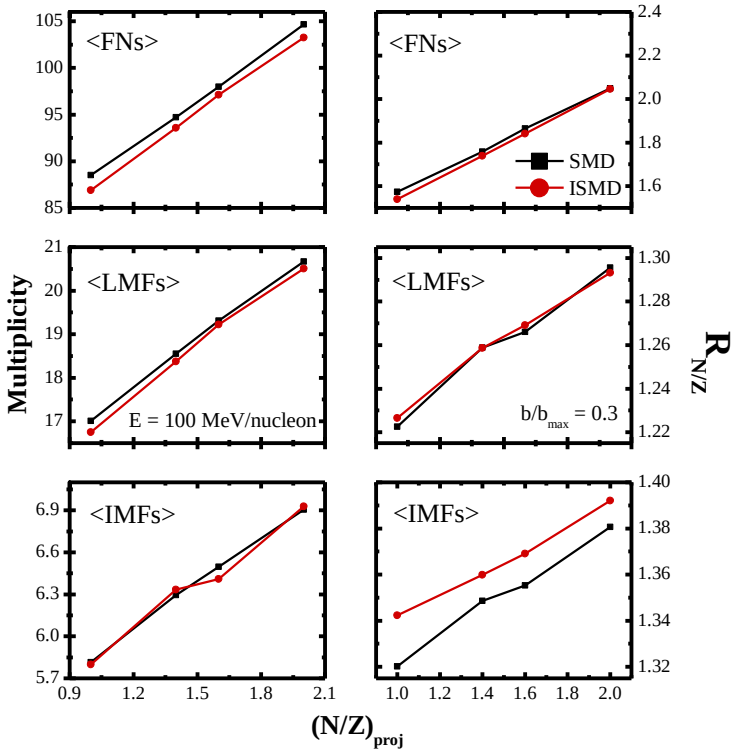

Fig.3.15 The dependence of multiplicity and $R_{N/Z}$ on the projectile neutron-proton ratio $(N/Z)_{Proj.}$

3.5 SUMMARY

In the present work, the role of SMD and ISMD interactions have been extensively studied in the multifragmentation of asymmetric reactions within the framework of IQMD and IQMD (Th01) model respectively. This study has been made for various asymmetric reactions in which the target nuclei is taken as gold $\left({}^{197}_{79}Au\right)$ and different projectile nuclei. The reactions are : ${}^{12}_{6}C+{}^{197}_{79}Au$ (η=0.8), ${}^{24}_{12}Mg+{}^{197}_{79}Au$ (η=0.7), ${}^{40}_{18}Ar+{}^{197}_{79}Au$ (η=0.6), ${}^{56}_{26}Fe+{}^{197}_{79}Au$ (η=0.5), ${}^{83}_{36}Kr+{}^{197}_{79}Au$ (η=0.4) and ${}^{131}_{54}Xe+{}^{197}_{79}Au$ (η=0.2), ${}^{40}_{20}Ca+{}^{197}_{79}Au$ (N/Z=1), ${}^{48}_{20}Ca+{}^{197}_{79}Au$ (N/Z=1.4), ${}^{52}_{20}Ca+{}^{197}_{79}Au$ (N/Z=1.6), ${}^{60}_{20}Ca+{}^{197}_{79}Au$ (N/Z=2.0). These reactions have been simulated at various incident energies and colliding geometries. The results clearly signifies the importance of ISMD in the dynamics of asymmetric reactions, while negligible role is played for symmetric reactions due to lower isospin asymmetry. The present work concludes that, ISMD should be considered while studying the various aspects of asymmetric reactions.

REFERENCES

[1] B.A. Li, L.W. Chen and C.M. Ko, Phys. Rep. **464**, 113 (2008).

[2] J. Schaffner and I. Mishustin, Phys. Rev. C **53**, 1416 (1996); H. Shen, Phys. Rev. C **65**, 035802 (2002); C. Ishizuka *et al*., J. Phys. G: Nucl. Part. Phys. **35**, 085201 (2008); K. Sumiyoshi, S. Yamada and H. Suzuki, J. Astrophys. **667**, 382 (2007); X. Campi *et al*., Phys. Rev. C **67**, 044610 (2003).

[3] K.E. Zyromski *et al*., Phys. Rev. C **55**, R562 (1997); L.C. Vaz, J.M. Alexander and G.R. Satchler; Phys. Rep. **69**, 373 (1981); M. Beckerman, Rep. Prog. Phys. **51**,1047 (1988); M.K. Sharma, Ph. D. Thesis, P. U. Chandigarh (1998).

[4] H. Stocker and W. Griener, Phys. Rep. **137**, 277 (1986)

[5] J. Aichlein *et al*., **37**, 2451 (1988).

[6] J. Aichelin *et al*., Phys. Rev. Lett. **58**, 1926 (1987).

[7] M. Demoulins *et al*., Phys. Lett. B **241**, 476 (1990).

[8] R. Ogul *et al*., Phys. Rev. C **83**, 024608 (2011).

[9] R. Donangelo and S.R. Souza, Phys. Rev. C **532**, 326 (1995).

[10] J.K. Dhawan and R.K. Puri, Phys. Rev. C **75**, 057601 (2007); B. Jakobbson *et al*., Nucl. Phys. A **509**, 195 (1990); J.P. Hubble *et al*., Z. Phys. A **340**, 263 (1991); A. Schuttauf *et al.*, Nucl. Phys. A **607**, 457 (1998); S. Hudden *et al.*, Phys. Rev. C **67**, 064613 (2003); A. Bohnet *et al*., Nucl. Phys. A **494**, 349 (1989).

[11] K.S. Vinayak and S. Kumar, Pram. J. Phys. **20**, 1 (2014); J. Singh, R.K. Puri and J. Aichelin, Phys. Lett. B **519**, 46 (2001); C. Sfienti *et al*., Nucl. Phys. A **749**, 83 (2005); M.D. Toro *et al*., Nucl. Phys. A **681**, 426 (2001); Sangeeta, A. Jain and S. Kumar, Nucl. Phys. A **927**, 220 (2014); S. Kumar and R.K. Puri, Phys. Rev. C **89**, 057603 (2014).

[12] V. Kaur and S. Kumar, Phys. Rev. C **81**, 064610 (2010).

[13] L.G. Moselto, D.N. Delis, G.J. Wozniak, Phys. Rev. Lett. **71**, 3935 (1993).

[14] L. Phair *et al*., Phys. Rev. Lett. **77**, 822 (1996).

[15] D.R. Bowman *et al*., Phys. Rev. Lett. **67**, 1527 (1991).

[16] J. Hubele *et al*. Phys. Rev. C **46**, R1577 (1992).

[17] Y.G. Ma *et al*., Phys. Rev. C **69**, 031604 (2004).

[18] D.V. Shetty *et al*., Phys. Rev. C **68**, 054605 (2003).

[19] N. Marie *et al*., Phys. Rev. C **58**, 256 (1998).

[20] R.T. de Souza *et al*., Phys. Lett. B **268**, 6 (1991).

[21] M.B. Tsang *et al*., Phys. Rev. Lett. **71**, 1502 (1993).

[22] L. Manduci *et al*., Nucl. Phys. A **811**, 93 (2008).

[23] C.A. Ogilvie *et al*., Phys. Rev. Lett. **67**, 1214 (1991); M.B. Blaich *et al*., Phys. Rev. C **48**, 610 (1993).

[24] A. Schüttauf *et al*., Nucl. Phys. A **607**, 457 (1996).

[25] C. William *et al*., Phys. Rev. C **55**, R2132 (1997).

[26] B. Jakobsson *et al*., Nucl. Phys. A **509**, 195 (1990).

[27] J.Y. Liu *et al*., Phys. Rev. C **63**, 054612 (2001).

[28] Y.K. Vermani and R.K. Puri, J. Phys. G: Nucl. And Part. Phys., **36**, 105103 (2009).

[29] J. Aichelin, Phys. Rep. **202**, 233 (1991).

[30] D. Sisan *et al*., Phys. Rev. C **63**, 027602 (2001).

[31] V. Kaur and S. Kumar, J. Phys. Conf. Ser. **312**, 082028 (2010).

[32] C. Hartnack *et al.,* Eur. Phys. J. A **1,**151 (1998); C. Hartnack *et al.*, Phys. Rep. **510**, 119 (2012).

[33] J. Singh, S. Kumar, R.K. Puri, Phys. Rev. C **63**, 054603 (2001).

[34] J. Singh, S. Kumar, R.K. Puri, Phys. Rev. C **62**, 044617 (2000).

[35] J.P. Bondorf *et al*., Phys. Rep. **257**, 133 (1995).

[36] P. Bonche, S. Koonin and J.W. Negele, Phys. Rev. C **13**, 1226 (1976).

[37] J. Aichelin *et al*., Phys. Rev. C **31**, 1730 (1985).

[38] H. Duarte, Phys. Rev. C **75**, 024611 (2007); S. Kumar and R.K. Puri, Phys. Rev. C **58**, 320 (1998).

[39] J.J. Molitoris, H. Stocker and B.L. Winer, Phys. Rev. C **36**, 220 (1987).

[40] J. Cugnon and C. Volant, Z Phys. A **334**, 435 (1989).

[41] E.A. Uehling and G.E. Uhlenbeck, Phys. Rev. C **43**, 552 (1933).

[42] B.A. Li and S.J. Yennello, Phys. Rev. C **52,** R1746 (1995).

[43] E. Lehmann et al., Phys. Rev. C **51**, 2113 (1995); H. Sorge, Phys. Rev. C **52**, 3291 (1995).

[44] N.K. Virk, K.S. Vinayak and S. Kumar, Proc. DAE Symp. Nucl. Phys. **58,** 310 (2013); K.S. Vinayak, N.K. Virk and S. Kumar, Proc. DAE Symp. Nucl. Phys. **58**, 336 (2013); A. Kaur and S. Kumar, Proc. DAE Symp. Nucl. Phys. **58**, 430 (2013).

[45] S. Kumar, S. Kumar and R.K. Puri, Phys. Rev. C **81**, 014611 (2010); S. Kumar, Rajni and S. Kumar, Phys. Rev. C **82**, 024610 (2010); A. Jain, S. Kumar and R.K. Puri, Phys. Rev. C **84**, 057602 (2011); K.S. Vinayak and S. Kumar, J. Phys. G: Nucl. Part. Phys. **39**, 095105 (2012); S. Gautam, J. Phys. G: Nucl. Part. Phys. **37**, 085102 (2010).

[46] G. Peilert *et al.*, Mod. Phys. Lett. A **3**, 459 (1988); R.K. Puri and S. Kumar, Phys. Rev. C **57**, 2744 (1998).

[47] S. Kumar and R.K. Puri, Phys. Rev. C **58**, 320 (1998); J. Singh and R.K. Puri, J. Phys. G: Nucl. Part. Phys. **27**, 2091 (2000).

[48] C. Gale *et al*., Phys. Rev. C **35**, 1666 (1987).

[49] L. Zhuxia, C. Hartnack, Phys. Rev. C **44**, 824 (1991).

[50] L.G. Arnold et al., Phys. Rev. C **25**, 936 (1982); G. Passatore, Nucl. Phys. A **95**, 694 (1967).

[51] S.W. Huang *et al*., Phys. Lett. B **298**, 41 (1993); J. Singh and R.K. Puri, Phys. Rev. C **65**, 024602 (2002); W. Zuo et al., High Eng. Phys. And Nucl. Phys**. 9**, 881 (2005); C.J. Yan *et al*., Chin. Phys. Lett. **24,** 76 (2007); P. Danielewicz, Nucl. Phys. A **673**, 375 (2000).

[52] S. Kumar and R.K. Puri, Phys. Rev. C **60**, 054607 (1999).

[53] B.A. Li *et al*., Phys. Rev. C **69**, 011603 (2004).

[54] G. Peilert, Phys. Rev. C **39**, 1402 (1989).

[55] S. Kumar and R.K. Puri, Phys. Rev. C **60,** 054607 (1999); J. Singh, S. Kumar and R.K. Puri, Phys. Rev. C **63**, 054603 (2001); Y.K. Vermani, S. Goyal and R.K. Puri, Phys. Rev. C **79**, 064613 (2009); S. Gautam and P. Bansal, Phys. Part. Nucl. Lett. **10**, 110 (2013).

[56] M. Berenguer *et al*., J. Phys. G: Nucl. Part. Phys. **18**, 655 (1992); J.Y. Liu *et al*., Phys. Rev. C **67**, 024608 (2003); S. Kumar and S. Kumar, Chin. Phys. Lett. **27**, 062504 (2010).

[57] J.Y. Liu *et al*., Chin. Phys. Lett. **22**, 65 (2005).

[58] L.J. Ye *et al*., Chin. Phys. **15**, 1738 (2006).

[59] B.A. Li *et al*., Phys Rev. C **69**, 011603(R) (2004).

[60] B.A. Li *et al*., Nucl. Phys. A **735**, 563 (2004).

[61] S. Kumar, S. Kumar and R.K. Puri, Phys. Rev. C **78**, 064602 (2008).

[62] W.J. Guo and J.Y. Liu, Chin. Phys. C **32**, 172 (2008); J.Y. Liu *et al*., Chin. Phys. **15**, 1738 (2006).

[63] J. Xu, L.W. Chen, C.M. Ko, and B.A. Li, Phys. Rev. C **81**, 055803 (2010).

[64] L.W. Chen, C.M. Ko , B.A. Li, and G.C. Yong, Front. Phys. China **2**, 327 (2007).

[65] C.B. Das, S. Das Gupta, C. Gale and B.A. Li, Phys. Rev. C **67**, 034611 (2003).

[66] K.S. Vinayak, Ph.D Thesis 2013, Thapar University, Patiala (India).

[67] D.T. Khoa *et al.*, Nucl. Phys. A **548**, 102 (1992); R.K. Puri *et al.*, Nucl. Phys. A **575**, 733 (1994); R.K. Puri et al., J. Phys. G: Nucl. Part. Phys. **20**, 1817 (1994).

[68] D. Polster *et al*., Phys. Rev. C **51**, 1167 (1995).

[69] M. Dzelalija *et al*., Phys. Rev. C **52**, 346 (1995).

[70] N. Marie *et al*., Phys. Rev. C **58**, 256 (1998).

[71] M. Colonna *et al*., Nucl. Phys. A **805**, 454 (2008).

[72] X.Y. Sun *et al*., Phys. Lett. B **682**, 396 (2010).

[73] J. Xu, Z. Martinot and B.A. Li, Phys. Rev. C **86**, 044623 (2012).

[74] N.K. Virk, R. Kaur and S. Kumar, Proc. 75-years of Nuclear Fission: Present Status and Future Perspectives, May 8-10, 2014, Pg. No. **110.**

[75] Role of isospin momentum dependent interactions in multifragmentation of mass asymmetric colliding nuclei, N.K. Virk, R. Kaur, S. Kumar, R.K. Puri and S. Bhattacharya (to be submitted)